Dynamics of core accretion

Mon. Not. R. Astron. Soc. **000**, 000–000 (0000) Printed 26 November 2012 (MN LATEX style file v2.2)

Dynamics of Core Accretion

Andrew F. Nelson[1⋆] and Maximilian Ruffert[2]
[1] *Los Alamos National Laboratory, XCP-2 MS T087, Los Alamos NM, 87545, USA*
[2] *School of Mathematics and Maxwell Institute, University of Edinburgh, Edinburgh Scotland EH9 3JZ*
E-mail: andy.nelson@lanl.gov (AFN); M.Ruffert@ed.ac.uk (MR)

Accepted 2345, February 31. Received 2346, February 32; in original form 2347, February 33

ABSTRACT

We perform 3-dimensional hydrodynamic simulations of gas flowing around a planetary core of mass $M_{\rm pl}$=10$M_\oplus$ embedded in a near Keplerian background flow, using a modified shearing box approximation. We assume an ideal gas behavior following an equation of state with a fixed ratio of the specific heats, $\gamma = 1.42$, consistent with the conditions of a moderate temperature background disk with solar composition. No radiative heating or cooling is included in the models. We employ a nested grid hydrodynamic code implementing the 'Piecewise Parabolic Method' with as many as six fixed nested grids, providing spatial resolution on the finest grid comparable to the present day diameters of Neptune and Uranus.

We find that a strongly dynamically active flow develops such that no static envelope can form. The activity is not sensitive to plausible variations in the rotation curve of the underlying disk. It is sensitive to the thermodynamic treatment of the gas, as modeled by prescribed equations of state (either 'locally isothermal' or 'locally isentropic') and the temperature of the background disk material. The activity is also sensitive to the shape and depth of the core's gravitational potential, through its mass and gravitational softening coefficient. Each of these factors influence the magnitude and character of hydrodynamic feedback of the small scale flow on the background, and we conclude that accurate modeling of such feedback is critical to a complete understanding of the core accretion process.

The varying flow pattern gives rise to large, irregular eruptions of matter from the region around the core which return matter to the background flow: mass in the envelope at one time may not be found in the envelope at any later time. No net mass accretion into the envelope is observed over the course of the simulation and none is expected, due to our neglect of cooling. Except in cases of very rapid cooling however, as defined by locally isothermal or isentropic treatments, any cooling that does affect the envelope material will have limited consequences for the dynamics, since the flow quickly carries cooled material out of the core's environment entirely. The angular momentum of material in the envelope, relative to the core, varies both in magnitude and in sign on time scales of days to months near the core and on time scales a few years at distances comparable to the Hill radius. The dynamical activity contrasts with the largely static behavior typically assumed within the framework of the core accretion model for Jovian planet formation.

We show that material entering the dynamically active environment may suffer intense heating and cooling events the durations of which are as short as a few hours to a few days. Shorter durations are not observable in our work due to the limits of our resolution. Peak temperatures in these events range from $T \sim 1000$ K to as high as $T \sim 3 - 4000$ K, with densities $\rho \sim 10^{-9} - 10^{-8}$ g/cm^3. These time scales, densities and temperatures span a range consistent with those required for chondrule formation in the nebular shock model. We therefore propose that dynamical activity in the Jovian planet formation environment could be responsible for the production of chondrules and other annealed silicates in the solar nebula.

Key words: hydrodynamics, planets: formation, planetary systems: formation

1 INTRODUCTION

The classical 'core accretion' model for Jovian planet formation (Wuchterl *et al.* 2000) is characterized by the idea that a 5–15 earth mass ($M_\oplus$) rock/ice core forms at a distance of ∼5 AU or more from the central star (Boss 1995), with a gaseous envelope surrounding it. At some critical point during the growth, the gaseous envelope becomes unstable and collapses, ultimately accreting as much as several times the mass of Jupiter.

In outline, the core accretion model consists of three distinct phases (Pollack *et al.* 1996). First, a sold core accretes from smaller solid bodies like comets and asteroids in the solar nebula. The mass of this core may be as much as 20-30 $M_\oplus$, depending on the model, though values of 5-15$M_\oplus$ are much more typically expected. The relatively rapid growth of this core is cut off when it depletes its 'feeding zone', at which point begins a much slower period of growth of both the core, from material migrating into the feeding zone from other parts of the disk, and of the surrounding hydrostatic gaseous envelope. In this second phase, the gas accretion rate is regulated by the balance of radiative cooling and the continued heating of the envelope by a low rate of solid body accretion. When the combined mass of the core and envelope reaches a (model dependent) critical value of $\sim 30M_\oplus$, the hydrostatic envelope becomes unstable and period of rapid gas accretion follows, defining the third, 'core instability', stage of evolution. The planet's final mass is determined during this phase.

The most critical problem afflicting the core accretion model is that the second stage may require as much as 6 million years or more (Pollack *et al.* 1996), but the circumstellar disk out of which the planet purportedly forms may have a lifetime of only 2-4 million years (Haisch *et al.* 2001). More critically, when the dynamical consequences of the interaction between the forming planet and disk are taken into account, the planet's lifetime may shrink to only a few $\times 10^4$ years before it migrates inwards toward the star and is accreted by it (see e.g. Ward & Hahn 2000, and references therein). While some migration is certainly necessary, since the vast majority of extra solar planets so far discovered have been observed in orbits less than (often much less than) the ∼5 AU where they are expected to form, the rates expected from theory would imply that no planets could outlive the disks in which they form.

1.1 Newer wrinkles in core accretion

Pollack *et al.* (1996) show that among the most sensitive input parameters for the formation time scale is how the planetesimal accretion rate varies with time, especially in the second phase of growth after the core has grown substantially and depleted its feeding zone. The cause of the sensitivity is the continued heating of the envelope gas by the solids as they pass through and are dissolved in the envelope when they accrete. The heating then stalls both further envelope contraction and gas accretion onto the core.

These models were performed in the context of a single, isolated core in a background disk where no other cores competed for the same resources and no migration through the disk occurred. The time scale can be shortened considerably when either assumption is relaxed. Alibert *et al.* (2004) have shown that including migration can shorten the required lifetime to $\lesssim$1Myr even in a much less massive disk than originally studied because, due to the migration the planet does not deplete its feeding zone for solid bodies. Instead, its heavy element core continues to grow rapidly, triggering runaway gas accretion much more quickly than otherwise. A possibly undesirable consequence of the model is that critical core mass is higher, perhaps in conflict with the data for the observed core mass of Jupiter.

Although not including migration, Hubickyj *et al.* (2005) have simulated the effects of competing embryos with a 'cutoff' of the solid body accretion when the core reaches a predetermined mass, modeling the fact that the solids at more than some critical distance from one core have been accreted by another. In addition, they study the sensitivity of their models to the treatment of opacity in the envelope, which governs the rate at which cooling of the envelope (followed by contraction and further accretion) can proceed. Previous studies have used opacities that are appropriate for interstellar grains and therefore do not properly model the processing expected during the evolution of the circumstellar disk and later the gaseous planetary envelope itself. Such processing, especially in the envelope, means that opacities will be reduced as grains coagulate and 'rain out' of the forming planet's upper envelope. Hubickyj *et al.* (2005) model such processing with a temperature dependent reduction of the interstellar opacity value and, coupled with the cutoff mass, find that the required formation time scale is reduced to as little as 1 Myr, with critical core masses of 5-10$M_\oplus$.

1.2 Shortcomings in the models and goals for this work

An important underlying assumption made in core accretion models is that a hydrostatic envelope structure exists, so that a one dimensional approximation may be used to reproduce the evolution. On the other hand, previous numerical studies of planets embedded in disks have shown that this hydrostatic assumption may not be realistic, even for very low mass cores. For example, D'Angelo *et al.* (2002) show that in 2D nested grid simulations, spiral structure exists in the circumplanetary disks of cores as small as $3M_\oplus$, and that for cores of $\gtrsim 10M_\oplus$ strong spiral shocks are present. Bate *et al.* (2003) perform similar simulations in 3D and also observe spiral structures and rotation, though they do not find shock structures as strong as in the 2D work. Their simulations implemented an isothermal equation of state however, which is certainly inappropriate for such dense regions as the envelope of a forming planet and may result in flows that do not reproduce the true picture of the evolution. Later work of Ayliffe & Bate (2009, hereafer AB09) relaxes the isothermal assumption in some of their simulations, instead using a flux limited radiative transfer model of a small cutout region of the disk whose evolution was simulated with a Smoothed Particle Hydrodynamics (SPH) code with a resolution of 3×10^4 SPH particles. Their conclusions are similar to the isothermal results in the sense that in both cases, spiral structures and/or envelope asymmetries develop, but are weaker in the radiative transfer models, and accretion rates onto the core are lower.

Although these studies are good first steps, to date

there has been little exploration of the region of parameter space between the two extremes of, at one end, detailed modeling of the disk with very coarse modeling of the core and envelope, and at the other, of detailed modeling of the core and envelope with coarse or non-existent modeling of the disk. The simulations of AB09 for example, which are among those with the highest claimed resolution of the region around the core, employ a total of only 3×10^4 or 1×10^5 (in different simulations) particles over the entire volume. In order to fully understand the core accretion scenario, detailed models of the flow around and onto the core at much higher resolution are necessary.

Models of accretion onto compact objects have been published (see e.g. Ruffert 1997, 1999, and references therein), and in many cases large scale instabilities in the flow develop Foglizzo & Ruffert (1999) that are often characterized by 'flip-flop' behavior in the sense that angular momentum accretion can temporarily switch sign. While 3D models produce uniformly less active flow than 2D models, both produce such behavior and in most cases, the accretion rate of various flow variables is comparable to the classical Bondi-Hoyle rate even in flows with transverse gradients.

The applicability of these models and their results to planet formation would appear to be quite limited however because they typically assume a central body which accretes matter with perfect efficiency (e.g. a 'black hole'). In the context of planet formation, the accretor is of course a rocky planetary core, onto which gas accretion is forbidden and an envelope structure develops. Moreover, while the background gas flow in previous studies may include some transverse velocity or density gradients, it is uni-directional. In contrast, the flow around a forming planet is quite complex, with a flow that circulates in opposite directions relative to the planet inside and outside its orbit, but which librates in a region near its orbit. The existence of the planet may drive complex interactions between each of the three regions and with planet's envelope as well.

With such large differences in the accretion assumptions and in the background flow pattern, will similar sorts of dynamical activity as in the simpler cases occur? How does the existence of dynamical activity (if indeed it is present) affect the time scale required for the core accretion model to succeed? In other words, can dynamical activity somehow short circuit the slow, near hydrostatic evolutionary process assumed in the second phase of planet growth, replacing it with a more rapid growth phase that avoids the problems of rapid Type I migration? Or does it instead lengthen the process?

The goal of this paper is to begin an investigation of the accretion process in order to determine the character of any dynamical activity that may occur. We will extend the previous comparatively low resolution, two and three dimensional calculations exploring planet migration to very high resolution three dimensional calculations specifically studying the mass accreting onto a $10M_\oplus$ core. The models in our study will consist of a small cubic 'cutout' region of a circumstellar disk and centered on the core. They will therefore not include migration of the planet itself, but will include some effects of the background on the accretion flow, such as the effects of different disk density and temperature distributions. In section 2 we define the physical conditions assumed in our models and numerical methods used to realize the evolution, as well as the initial conditions we implement for our numerical models. Section 3 contains the basic results of our simulations and introduces some metrics by which those results may be compared more quantitatively. Section 4 expands on these analyses with further studies of the sensitivity of the results to various parameters. Finally, section 5 proposes a potential link between the dynamical activity around a forming Jovian planet and the formation of chondrules. Our concluding remarks are found in section 6, where we summarize our conclusions and the implications they have for Jovian planet formation and compare our results with previous work. Finally, in section 7, we discuss a number of questions that may be profitably addressed by future work similar to our own.

2 THE PHYSICAL MODEL

In this section we describe the physical models we use to study the flow pattern of gas around the forming planetary core, the numerical code used to evolve the models forward in time and the initial conditions of those models. Our study will include or exclude a variety of physical properties of the system in different simulations. Therefore we will outline the most physically inclusive models, and in later discussion note specifically which properties have been included in which simulation. In general, the properties we study are either substitutive, eg. either one equation of state or another, or cumulative, e.g. gravity from different components of the system, so that separate, excluded components can simply be neglected in the specification of the initial state.

2.1 The mathematical framework, numerical realization and physical assumptions

In previous works studying disks, it has been customary to implement either a fully curvilinear coordinate system (usually cylindrical) or a 'shearing sheet' approximation. The latter form is an approximation in which locally Cartesian coordinate system is used rather than the full equations for curvilinear coordinates which simplifies the analysis, especially in the context of linearized instability analyses. It neglects most of the non-uniform geometric features of the coordinate system and instead adds a number of terms to model approximately some of its effects, and the rotation of the coordinate frame itself.

We have implemented neither procedure here, but rather an intermediate step between them which we call a 'modified shearing sheet' coordinate system. As does the standard shearing sheet coordinate system, this modified shearing sheet system neglects the geometric terms in the full curvilinear system of equations. Its main difference from the standard form is that it retains a more precise treatment of the gravity and fictitious forces on the gas, as noted below. Due to our somewhat unusual treatment of the coordinate system, we shall describe here in some detail both the derivation of the background analytic and numerical frameworks, as well as the initial and boundary conditions used in our models.

2.1.1 Mapping cylindrical to modified shearing sheet coordinates

Like the shearing sheet, our mathematical formalism requires that the true cylindrical coordinate system be mapped onto a Cartesian coordinate system centered on the planet. We define the mapping so that the three pairs (x, r), (y, $r\phi$) and (z, z) each correspond as follows. Mapping the cylindrical coordinates of the disk to the Cartesian coordinates of our grid requires the three identifications

$$x = r - a_{\rm pl}; \quad y = r\phi; \quad z = z \tag{1}$$

with $a_{\rm pl}$ defined as the semi-major axis of the planet. This identification means that each x grid coordinate is defined to be at the same distance from the star even though this condition would not be true for a true Cartesian grid centered on the planet. The errors that are made by such an identification will be small as long as the extent of the coordinate grid itself is small, compared to the distance to the origin.

In our models, we typically simulate the gas flow in a region $\sim$ 0.45 AU (4 'Hill radii' from a $10M_\oplus$ object) in each coordinate direction from a point centered 5.2 AU away from the origin. In a cylindrical coordinate system, two 'cubic' volume elements at the inner and outer edges of a grid of this size (i.e. $rdrd\phi dz$, with each side of the volume identical in length) will differ in actual volume by a factor ~ 1.4, whereas in our Cartesian coordinate system they will be equal. Because the flow is largely azimuthally directed, very little gas will undergo (or fail to undergo in our coordinate system) expansion or contraction by such a factor and therefore only small errors will develop from this source.

2.1.2 The equations of hydrodynamics

Here we state explicitly the fully expanded form of the equations we solve. The hydrodynamic variables for mass, momentum and energy conservation are defined with the usual symbols with ρ referring to the mass density, v_x, v_y and v_z to the velocities in each of the three coordinate directions and $E = \rho(u + v^2/2)$ to the total energy, where v is the magnitude of the total velocity and u is the specific internal energy.

The continuity equation for mass conservation is given by

$$\frac{\partial\rho}{\partial t} + \frac{\partial(\rho v_x)}{\partial x} + \frac{\partial(\rho v_y)}{\partial y} + \frac{\partial(\rho v_z)}{\partial z} = 0, \tag{2}$$

and the equations of motion in the three Cartesian directions are given by

$$\frac{\partial(\rho v_x)}{\partial t} + \frac{\partial(\rho v_x v_x)}{\partial x} + \frac{\partial(\rho v_x v_y)}{\partial y} + \frac{\partial(\rho v_x v_z)}{\partial z} - \frac{\rho V_y^2}{a_{\rm pl}+x} = -\frac{\partial p}{\partial x} - \rho\frac{\partial\Phi}{\partial x}, \tag{3}$$

$$\frac{\partial(\rho v_y)}{\partial t} + \frac{\partial(\rho v_y v_x)}{\partial x} + \frac{\partial(\rho v_y v_y)}{\partial y} + \frac{\partial(\rho v_y v_z)}{\partial z} + \frac{\rho v_x v_y}{a_{\rm pl}+x} + 2\frac{\rho v_x V_y}{a_{\rm pl}+x} = -\frac{\partial p}{\partial y} - \rho\frac{\partial\Phi}{\partial y} \tag{4}$$

and

$$\frac{\partial(\rho v_z)}{\partial t} + \frac{\partial(\rho v_z v_x)}{\partial x} + \frac{\partial(\rho v_z v_y)}{\partial y} + \frac{\partial(\rho v_z v_z)}{\partial z} = -\frac{\partial p}{\partial z} - \rho\frac{\partial\Phi}{\partial z}. \tag{5}$$

For models in which an equation for the conservation of energy is required (i.e. models without locally isothermal or locally isentropic equations of state), the energy conservation equation is

$$\frac{\partial E}{\partial t} + \frac{\partial(v_x(E+p))}{\partial x} + \frac{\partial(v_y(E+p))}{\partial y} + \frac{\partial(v_z(E+p))}{\partial z} = -\rho\left(v_x\frac{\partial\Phi}{\partial x} + v_y\frac{\partial\Phi}{\partial y} + v_z\frac{\partial\Phi}{\partial z}\right). \tag{6}$$

In equations 3 and 4 above, V_y is defined as

$$V_y = v_y + (a_{\rm pl} + x)\Omega_{\rm pl} \tag{7}$$

where $\Omega_{\rm pl}$ is the orbital angular velocity of the planet. V_y corresponds to the total azimuth velocity in a non-rotating cylindrical coordinate frame. An equation of state for the gas closes the system of equations and is described in section 2.1.3. The form of the total gravitational potential, Φ, is discussed in section 2.1.4, below.

Note that the above set of equations include no explicit contribution due to any viscous properties of the fluid. Such effects are well known to be present in the background circumstellar disk, with their origin commonly ascribed to turbulence generated by the so-called Magneto-Rotational instability (Balbus, Hawley & Stone 1996). Both the spatial and time scales relevant for this source of dissipation are inapplicable to the immediate environment of a core embedded in a circumstellar disk however, and we therefore neglect turbulence as a source of dissipation in our simulations. We similarly neglect other, less specific, sources of dissipation in favor of modeling only those characteristics of the flow to which we can define explicitly. Coupled with our numerical code (section 2.1.5), which itself contributes little dissipation to its solution of the flow equations, our simulations will therefore be highly inviscid. The only significant sources of dissipation will originate in shocks that develop in the flow, which the numerical scheme is known to handle well.

For reference, we point out the differences between our treatment and both the fully curvi-linear coordinate system and the shearing sheet, in Appendix A.

2.1.3 The thermodynamic treatment of the gas

The system of hydrodynamic equations are closed assuming an ideal gas equation of state given by:

$$p = (\gamma - 1)\rho u \tag{8}$$

where γ is the ratio of specific heats and p, ρ and u are respectively the pressure, density and specific internal energy of the gas. In order to derive the global initial condition for our simulations, we employ a vertically integrated (2D) equation of state of the form:

$$P = (\gamma - 1)\Sigma u \tag{9}$$

where P and Σ are the vertically integrated pressure and the mass surface density respectively. This form is exactly

analogous to that used in 3D for the simulations themselves, so that no adjustments to the rotation curve or any other quantities are required to establish a steady state initial condition. Finally, the sound speed and temperature are related by the equation

$$c_s^2 = \frac{\gamma RT}{\mu} \tag{10}$$

where R is the gas constant and $\mu = 2.31$ is the mean molecular weight of a gas of solar composition.

The choice of γ is not obvious in the range of temperatures and densities we study because in various regimes, some or all of a number of internal molecular states may be important. In order to avoid such complications, we assume that the gas is of solar composition with an effective single component accounting for both hydrogen and helium, so that the value for $\gamma = 1.42$. This value implies that the rotational degrees of freedom in hydrogen gas are active (corresponding to gas temperatures $\gtrsim 100$ K) but its vibrational degrees of freedom are inactive (corresponding to temperatures $\lesssim 800 - 1000$ K), and will be most representative of moderate temperature regions of the disk expected throughout most regions of our simulations.

Apart from heating from hydrodynamic processes like PdV work and shocks, we impose no other assumptions regarding the heating and cooling processes that are active in the disk. Of particular importance in this regard is our neglect of radiative heating and cooling, which will undoubtedly modify the behavior of the models to some extent. As a first, crude attempt to model such effects, we also perform a number of simulations using either a locally isothermal or locally isentropic equation of state, defined respectively as

$$p = \rho c_s^2 \tag{11}$$

and

$$p = K\rho^\gamma \tag{12}$$

with the value of γ set to 1.01 or 1.42 for the locally isothermal or locally isentropic cases respectively. The physical interpretation these equations of state in terms of their implications for heating and cooling are discussed in Nelson *et al.* (2000) and Pickett *et al.* (2003). The values of c_s^2 and K are set by the initial conditions of the simulation and are thereafter fixed for its duration. As with the ideal gas case, vertically integrated forms are employed to determine the global initial condition, prior to the beginning of the actual simulation.

2.1.4 The treatment of gravity

Gravity from the central star, from the planet core and from the circumstellar disk are included in our simulations. The contribution from the disk is further split into two parts, representing the portion of the disk inside and outside the simulation box.

The total gravitational potential is defined as a sum of several components from the star Φ_*, the planet $\Phi_{\rm pl}$, the background disk Φ_D, and the mass inside our simulation cube $\Phi_{\rm loc}$ as:

$$\Phi = \Phi_* + \Phi_{\rm pl} + \Phi_D + \Phi_{\rm loc} - \Phi_{\rm loc}^0. \tag{13}$$

The last term, $\Phi_{\rm loc}^0$, describing the initial value of the local gravitational potential due to material in the simulation cube, is required to avoid double counting disk mass that is otherwise computed in both the background disk and then again locally in the simulation cube, as we discuss in more detail below.

We assume that the central star is fixed at all times during our simulations, which means that its contribution to the gravitational force on the gas is constant. The gravity from the planetary core is also fixed in time, relative to the grid. Both the star and the planet are modeled as softened point masses with a softening that is similar in form to a Plummer law (Ruffert 1994) with a potential given by

$$\Phi = \frac{-GM}{(r^2 + \epsilon^2\delta^2 \exp[-r^2/\epsilon^2\delta^2])^{1/2}} \tag{14}$$

where G is the gravitational constant and the quantities Φ and M are replaced by with variants subscripted for the star or the planet planet as appropriate. The softening parameter ϵ is a tunable constant multiplying the grid spacing δ, and in our simulations is set to unity. The exponential term in the denominator causes the softening to decrease to zero at distances of more than a few grid spacings from the point mass, where it is not needed.

The distances, r, between the star or planet and each individual grid cell are determined from the grid spacing itself, with one important modification. In order to simplify our initial condition (see section 2.2.2), we neglect the y and z components of stellar gravity, so that the distance from the star to any point in the grid includes only the x component, effectively treating the x coordinate (plus the offset, $a_{\rm pl}$, defining the planet's semi-major axis in the underlying circumstellar disk) as a radial coordinate. The planet's contribution includes all three Cartesian components of the force.

The gravitational potential of the disk is split into two components, one from the disk as a whole (the 'global' component), and a second from the portion of the disk included in our cubic cutout region (the 'local' component). The global disk self gravity is computed once for the initial state, and thereafter remains constant for the duration of the simulation. The local potential is dependent on the time dependent flow through the disk and must therefore be recomputed at each time step.

We calculate the global component from the specified global mass distribution of the disk (see 2.2.1 below) using a Fourier transform based gravitational potential solver in cylindrical coordinates (see e.g. Binney & Tremaine 1987). Although the disk is axisymmetric, so that we would expect that a one dimensional solution for the potential with such a solver would be adequate, we have found that in practice this solver requires that a number of azimuth cells be used in order to converge to a well determined potential value. As discussed in section 2.2.1 below, the radial grid for our global initial condition requires as many as approximately 30000 cells for our highest resolution models. We have found that with this radial resolution we require at least 1024 azimuth grid cells be included in the potential solver to produce a potential solution that is accurate to numerical double precision (i.e. one part in $\sim 10^{15}$) over the entire radial range of 0.5 to 20 AU included in the global initial condition. Although we have made no specific investigation of the reasons

for the required number of azimuth cells, it seems likely to be due to the existence of a small self-contribution to the potential as obtained from the Fourier transform technique in cylindrical coordinates (Masset 1997), for which we attempted no correction. As for the stellar gravity, the background disk gravity is mapped to the x coordinate only.

The gravitational potential of material on the grid, $\Phi_{\rm loc}$, is determined from the Poisson equation

$$\left(\frac{\partial^2}{\partial x^2}+\frac{\partial^2}{\partial y^2}+\frac{\partial^2}{\partial z^2}\right)\Phi_{\rm loc}=4\pi G\rho. \tag{15}$$

We compute its value at each time using a 3D Cartesian coordinate FFT based potential solver. Due to the nested grid structure and the inclusion of the global disk potential there are two additional complications regarding the calculation of the potential that do not occur in the standard method of solution on a single grid. Both complications can be circumvented by straightforward application of the fact that the Poisson equation is linear, so that separate terms may be added and subtracted independently.

The first complication is that the potential calculation on each of the nested grids require contributions from mass outside of the sub-cube on which the potential is to be calculated. Ruffert (1992), notes that the full potential can be obtained from a sum of the contribution from a given fine grid, and from a second potential calculation that is performed on the overlying coarse grid, in which the mass on the finer grid is temporarily deleted. The portion of this second potential (on a given coarse grid) that overlaps the fine grid is mapped onto that fine grid as a background term and summed with the fine grid computation to obtain a correct final value.

The second complication arises because the global gravitational potential of the disk accounts for the contribution due to mass located both inside and outside of our local simulation box. This means that simply adding the contribution from the mass distribution within the simulation box would result in that matter being accounted for twice in the net gravitational potential. To determine the correct local potential, we first compute the gravitational potential of matter in the box due to the mass distribution of the initial state and save this value for the life of the simulation. The initial contribution is subtracted from the potential calculated at all later times, so that effectively only the difference in the mass distribution of the later and initial states is accounted for in the local potential and the double counting is avoided.

2.1.5 The numerical code

To model the flow at the extremely high spatial resolution required we have modified the code of Ruffert (1992). This code is based on the 'Piecewise Parabolic Method' (PPM) of Colella & Woodward (1984), in which a high order polynomial interpolation is used to determine cell edge values used in calculating a second order solution to a Riemann problem at each cell boundary. The interpolation is modified in regions of sharp discontinuities to track shocks and contact discontinuities more closely and retain their sharpness, while a monotonizing condition smoothes out unphysical oscillations. The solution to the one-dimensional Riemann problem is then used to calculate fluxes and advance the solution in time. Since the Riemann problem solution explicitly models the physical dissipation present in shock structures, no artificial viscosity is required for stability of the code, and none is included.

This code solves the hydrodynamic equations on a three dimensional Cartesian grid, and includes the possibility of including a series of statically generated nested grids. Each grid contains an identical number of zones in each of the three coordinate directions, but the grid spacing decreases by a factor of two when proceeding from a coarse to fine grid.

We have modified the original, strictly Cartesian code to account for centrifugal and Coriolis forces required in a coordinate system rotating with the planet core, but have neglected terms required to reproduce a fully curvi-linear coordinate system, as noted in section 2.1.2, above. This approximation will remain valid so long as the region modeled is relatively small, so that the curvature is unimportant.

Depending on the simulation (see table 1 below), between three and six nested grids each with 64^3 zones are used to model a cubic region around the planet. Successively finer grids have the same number of zones, but half of the linear dimensions of the immediately coarser grid and are also centered on the planet. When the simulation volume is defined by a region ± 4 Hill radii (section 2.1.6) around a $10M_\oplus$ planet, the linear resolution on the finest grid of our highest resolution models (6 nested grids) is $\delta x \approx 6.5\times10^9$ cm in size, about 30% larger than the diameter of Neptune or Uranus and the spatial volume is resolved with a total of approximately 1.4 million zones.

2.1.6 The Hill and accretion radii

In the discussion throughout this paper, two quantities will appear repeatedly, and so we introduce them here. They are the accretion radius of the planet core, defined as

$$R_{\rm A}=\frac{GM_{\rm pl}}{c_s^2} \tag{16}$$

and its Hill radius

$$R_{\rm H}=a_{\rm pl}\left(\frac{M_{\rm pl}}{3M_*}\right)^{1/3} \tag{17}$$

where G is the gravitational constant, $M_{\rm pl}$ and M_* are the mass of the planet core and the central star, respectively, $a_{\rm pl}$ is the semi-major axis at which the core orbits the star and c_s^2 is the square of the sound speed of the gas in the unperturbed (initial) disk near the core.

Taken in its original context of the Bondi accretion model, the accretion radius defines the distance from the core at which the magnitude of the internal energy of an isothermal gas and its gravitational potential energy become comparable. It therefore represents a measure of the spatial scale over which exchanges between the fluid's thermal energy and energy bound up in the bulk kinetic motion derived from its infall onto the core might be expected to lead to dynamical activity. Together with the mass of the core, the background temperature, through its presence in the relation for the sound speed, completely specifies the accretion radius.

The Hill radius defines another spatial scale of interest. Its value is derived from the Jacobi integral, a quantity which plays a role similar to the total energy in other (in-

ertial) systems, and which is the only conserved quantity in the restricted three body problem. It relates the gravitational potential energies imposed by the core and star on a test particle with that particle's kinetic energy as it travels through the combined system and a fourth 'centrifugal potential' term quantifying the effects of the non-inertial reference frame assumed for the system. It also defines the inner and outer extents of the Roche lobe of the planet, which is the full 3D volume around the core for which the combined gravitational influences of the core and star are comparable to the influence of the fictitious forces arising from the rotating reference frame.

2.2 Initial conditions

We develop the initial conditions for our simulations in a two stage process. First, we define a set of global conditions that describe an entire circumstellar disk in two spatial dimensions (r, ϕ). From these conditions, we extract a three dimensional cubic 'cutout' region centered on a point mass, assumed to be embedded within the disk. This dual specification requires a small note of clarification for readers, in that in various places throughout the text, 'mass density' might refer to either a mass per unit area, or to a mass per unit volume. While in most contexts the distinction will be clear, we will typically refer to each as either 'surface' or 'volume' density, respectively.

2.2.1 The Global Model

The initial conditions are developed from a global model of an accretion disk quite similar in morphology to the disks modeled in Nelson & Benz (2003). Specifically, we assume that a point mass representing the central star is surrounded by a circumstellar disk, whose inner and outer radial dimensions are $R_i = 0.5$ AU and $R_o = 20$ AU.

The mass in the disk is distributed according to a surface density power law of the form

$$\Sigma(r) = \Sigma_{\rm pl} \left(\frac{a_{\rm pl}}{r} \right)^p, \tag{18}$$

with a similar power law for temperature taking the form

$$T(r) = T_{\rm pl} \left(\frac{a_{\rm pl}}{r} \right)^q. \tag{19}$$

$\Sigma_{\rm pl}$ and $T_{\rm pl}$ are the surface density and temperature at the assumed orbit radius, $a_{\rm pl}$ of the planet, respectively. The power law exponents are ordinarily set to $p = q = 1.0$. In order to study the sensitivity of our results to the mass and temperature distributions however, we have also performed simulations with other exponents as well (see table 1).

The surface density coefficient is set to $\Sigma_{\rm pl} = 500$ g/cm^2. This value is somewhat smaller than that implied by the Pollack *et al.* (1996) model, for which 6 Myr were required to grow a Jovian mass planet. It is chosen so as to be consistent with the minimum mass solar nebula (MMSN), given the dimensions of the disk we assume. With the given spatial dimensions of the disk this surface density implies a disk mass of $M_{\rm D}$=0.0358$M_\odot$, comparable to the traditional MMSN value, but well below the $M_{\rm D} \sim 0.1-0.14 M_\odot$ required for the classical core accretion model (Pollack *et al.* 1996) to produce a fully formed Jovian planet within $\sim$ 6Myr.

The temperature exponent value of $q = 1$ is chosen to ensure that the scale height of the disk is approximately constant. It is steeper than the value usually expected from observations of circumstellar disks (e.g. Beckwith *et al.* 1990), but over the limited radial range we simulate, we do not expect the temperature gradient to play a large role. The principle benefit of choosing this value will be to simplify the correspondence between the global and local disk models, as discussed below. The temperature scale is set to $T_{\rm pl} = 200$ K, comparable to (but slightly warmer than) the ice condensation temperature expected to be important for the rapid coagulation of grains that begins the planet formation process. With this background temperature, the derived isothermal scale height of the disk, $H = c_s/\Omega$, normalized by the distance from the star is $H/r = 0.08$, as shown in figure 1.

We map each of the thermodynamic quantities onto a radial grid in cylindrical coordinates, equally spaced in $\ln(r)$. In order to ensure the most precise initial condition for each sub-grid, the local initial conditions are derived separately for each sub-grid. The grid spacing of the 1D global grid is adjusted at each derivation to be equal to the spacing of the current local grid. This means that over the full extent of the disk (0.5 to 20 AU) we require as many as 30000 radial grid points to determine the global initial condition. Since the global initial condition is determined only at the beginning of the simulation, used to determine a corresponding local condition and thereafter discarded, such high resolution poses a negligible cost in terms of the total time required for the simulation.

From the predefined temperature, surface density and equation of state, we determine a pressure gradient for the disk. The pressure gradient is then used in conjunction with the gravitational forces from the star and disk to determine a rotational velocity, under the assumption that radial accelerations due to pressure gradients, stellar and global disk self gravity and centrifugal forces exactly cancel each other and no radial motion exists. No initial perturbations are assumed in any of the models.

Finally, we combine the various quantities from our specification of the global disk conditions together to calculate a value of the Toomre Q parameter, defined as:

$$Q = \frac{\kappa c_s}{\pi G \Sigma}, \tag{20}$$

where κ is the local epicyclic frequency and c_s is the sound speed. Theoretically (see e.g. Binney & Tremaine 1987), values of $Q < 1$ define the conditions for which self gravitating, axisymmetric instabilities in disks are unstable to linear perturbations. Numerical simulations (e.g. Nelson *et al.* 1998; Pickett *et al.* 1998) have shown that self gravitating spiral instabilities can still grow for values $Q \lesssim 2-3$, but that disks with higher values are stable.

The conditions assumed for most of our simulations ensure the global stability of the disk to large scale self gravitating disturbances, as measured by the value of its Q parameter. However, in several simulations we will also study disks with background temperatures as low as $T_{\rm pl}$ =50 K. Since, in the context of a global initial condition, the value of Q in such a disk would certainly fall to values low enough (in the outer disk) to allow instabilities to grow so that other planet formation mechanisms to proceed, such values may seem rather unphysical or at least irrelevant. The simula-

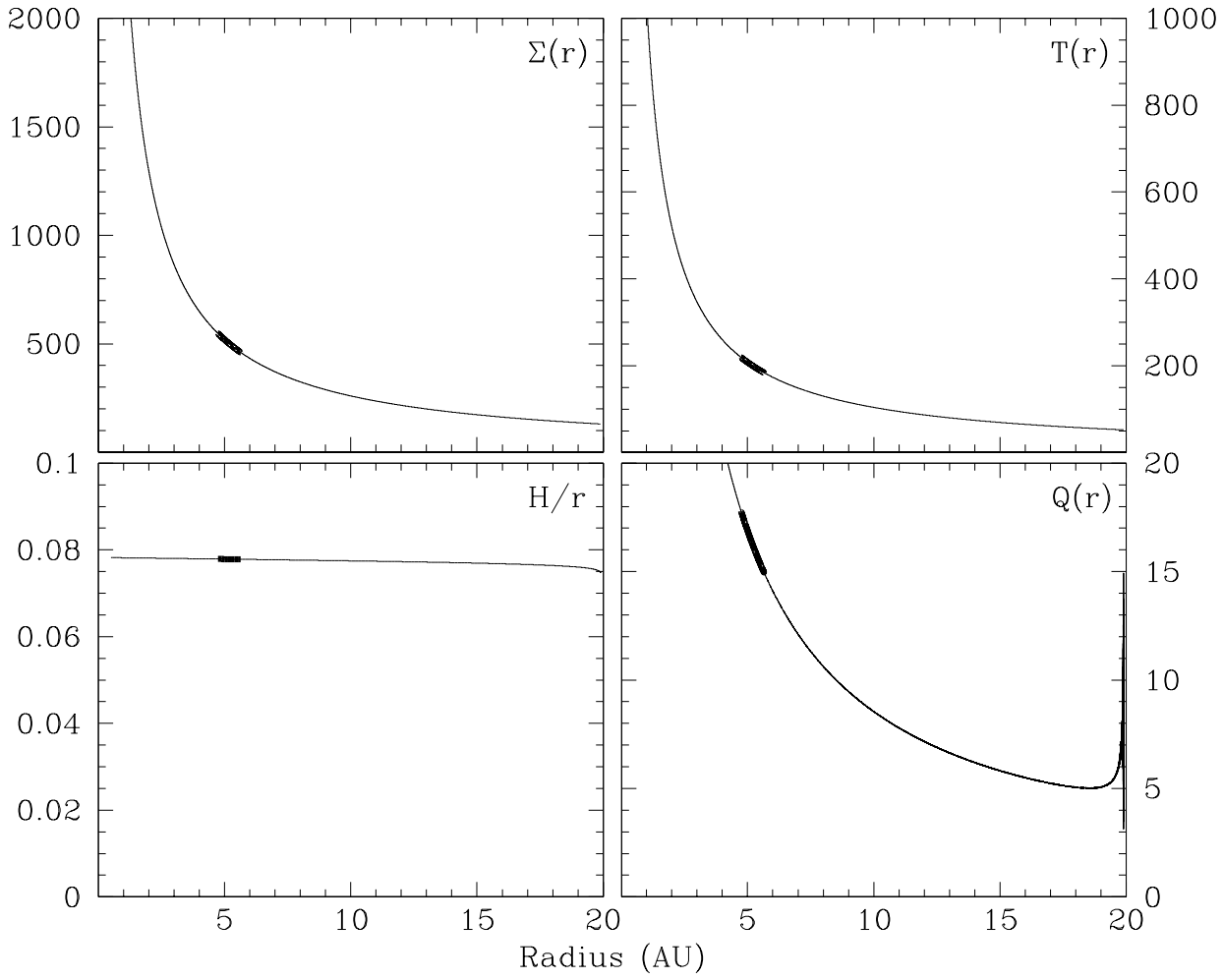

Figure 1. Global initial conditions for the disks underlying our simulations. Clockwise from the top left, the four panels of the image are the disk surface density, the temperature, the Toomre Q value and the dimensionless scale height. The heavy portion of each line corresponds to the portion of the initial condition considered in deriving the local initial condition.

tions remain interesting however because of their importance in outlining the behavior of the flow as a function of the ratio between the Hill and accretion radii, which we will find is an important measure of the dynamical activity in the flow.

A graphical summary of the global initial conditions for our prototype model (discussed in section 3.1 below) is shown in figure 1. As indicated, the lower right panel shows the Toomre stability parameter, Q, value for the simulations at each radius. Because $Q > 5$ for all radii, we expect that although global self gravity is included, self gravitating disk instabilities would not develop in the background flow, validating our assumption that it remains smooth. Disk self gravity remains important to consider however, first because, from a global perspective, it shifts the position of the corotation resonance relative to the planet, and second, from a local perspective, because we do not wish to discount the possibility that self gravitating instabilities could develop in the forming planet's envelope, even if they would not in the disk as a whole.

2.2.2 The Local Model

We use the global initial condition to derive the local initial condition inside our simulation cube in the following manner. First, we assume a planet core (modeled as a point mass) is embedded in the disk and orbits the star at a distance of $a_{\rm pl} = 5.2$ AU. Its orbit velocity is determined from the assumption that its orbit is circular and that it is affected by the gravitational forces from the star and from the disk. The planet's mass is set to $10M_\oplus$ and no accretion onto the core is allowed. The core is placed at the corner of eight adjacent grid zones which are not treated specially in any way, so that the core itself is effectively unresolved by the grid. We assume that no circumplanetary envelope exists around the core in the initial state, so that initial state is defined by the background flow, unperturbed by the planet. In order to allow the later flow to adapt more gracefully to this condition, we begin with a core mass of $1M_\oplus$ and allow it to grow linearly with time to its final mass over the course of the first 10 years of evolution. We have not observed any side

effects of this adjustment over the rest of the simulation's lifetime.

The simulation cube is centered on the core and is comoving with it. The dimensions of the cube are set to $\pm 4R_{\rm H}$ in each direction, corresponding to a cube of size ~ 0.897 AU on each side. In order to explore sensitivity to the core mass, we have performed one simulation with the core mass set to $20M_{\oplus}$, and we have performed several others with the cube volume as large as $\pm 6R_{\rm H}$, depending on the goals of the simulation. Table 1 below defines the initial parameters for each simulation.

The value of the x and z velocities (v_x and v_z–each set initially to zero), corresponding to the radial and vertical velocities of the global initial condition, and the internal energy of the gas are mapped directly from the global initial condition onto the local condition. Since the grid spacing of the 1D global initial state is preset to be identical to that on the corresponding 3D local grid, no interpolations are necessary. The values for the y velocity and volume density ρ require additional specification to complete the mapping from global to local.

The local y velocity is set from the global azimuth velocities of the gas in the disk and the planet core. Because we assume a simulation cube that is fixed relative to the core, in order to obtain the y velocity, we must first subtract off the angular velocity of the frame

$$v_y = V_\phi - (a_{\rm pl} + x)\Omega_{\phi \rm pl} \tag{21}$$

where V_ϕ is the orbit velocity of disk matter at each orbit radius and $\Omega_{\phi \rm pl}$ is the orbit velocity of the planet (and the rotation rate of the reference frame), and x is the offset from the planet's radial position, $a_{\rm pl}$.

The volume density remains to be determined. In a complete model of a circumstellar disk, we expect to find gradients of most of the hydrodynamic quantities in both the radial direction and in the z direction, due to the near Keplerian character of the disk and to the radiative heating and cooling processes acting on it. In order to simplify our study however, we have chosen to neglect the z component of both stellar gravity and global disk self gravity, so that effectively no vertical structure in the disk exists. The symmetry is broken only by the planet's gravitational force so that the flow around the core remains fully three dimensional.

Since the global initial condition is defined by a surface density rather than a volume density, we require a conversion to completely specify the local condition. For this conversion we introduce the small inconsistency in our models that we use an estimate of the disk scale height (which of course depends on the existence of the z component of stellar and disk gravity), and the relation $\rho = \Sigma/H$ to specify the correspondence. The scale height is in turn defined by $H = c_s/\Omega$ and Ω is the local rotation velocity in the disk. Its value of ~ 0.4 AU at the assumed orbit radius of 5.2 AU is approximately identical to the distance from the core to the edge of the simulation cube.

2.3 Boundary Conditions

In the shearing box formalism, the principle underlying the choice of boundary conditions is that no location in a disk is different than any other, excepting only that a shear term due to the background Keplerian motion must be accounted for explicitly. The box itself therefore represents one of many, essentially identical, replicas of a small subvolume of that disk. In this context, the common choice of implementing periodic boundary conditions for the shearing box (see e.g. Hawley, Gammie & Balbus 1995) means that a simulation of one small subvolume will be sufficient to represent the evolution of the entire disk. Clearly this principle does not hold for the present case, where our simlation volume contains a core and is therefore unique.

Instead, we implement a slighly more restrictive principle. Namely, we assume that the underlying disk background state is unchanging and is not affected by changes inside our simulation volume. We therefore set values for each state quantity in the boundary zones of the x and y coordinate directions of the local model (corresponding to the radial and azimuthal directions in the disk) to the initial values determined from the global model in the same manner that they would be had they instead been included in the simulation volume itself.

For the y boundaries, the conditions are fixed to their initial values for the duration of the simulation. Because the simulation volume is assumed to be a cutout taken from a circumstellar disk, the y boundary quantities are not identical at different x positions in the simulation, since they include the radial gradients of density, temperature and the rotation curve. This is an important consideration because at different x locations on the same boundary surface of the simulation box, corresponding to different orbit radii in the underlying circumstellar disk, y velocities may be directed either into or out of the simulation volume, with differing magnitudes. This behavior is a consequence of the initial near Keplerian flow of the underlying disk model, for which the y velocity varies as a function of the x position relative to the planet.

Boundary conditions in the x coordinate are set assuming the same fixed initial condition. Flow into the grid is permitted but the value of each hydrodynamic quantity (including v_x, the velocity perpendicular to the boundary) is reset to its initial value at each time step, so that the assumption of a fixed background state is maintained. Flow out of the grid is also allowed, should conditions require, by allowing v_x to take on either zero or the value just inside the boundary if that velocity is directed outwards.

This condition compensates for the development of large scale 'wakes', in the flow, corresponding to spiral structures in the underlying circumstellar disk, which include some radial motion directed away from the planet in each direction. If a completely fixed condition is implemented, such structures can be reflected strongly and unphysically back into the simulation volume. Some reflection still occurs with the limited outflow condition, although at the level it is present, it proves essentially harmless because the amount of reflected material is both small and is quickly carried out of the grid through the y boundary.

Initial simulations of mass propagating through simulation cube not containing a planet core demonstrated that inflow/outflow boundaries in the z coordinate resulted in large scale eddies forming in the flow. In order to avoid this problem, we use a reflecting condition on the z boundaries instead. Employing this condition together with the ones for the x and y directions resulted in a quiescent flow throughout the simulation volume for as long (several hun-

dred years) as we cared to follow the evolution, and we did not pursue the origin of the eddies further.

3 RESULTS OF SIMULATIONS

Using the initial conditions and physical models described above we have performed a number of numerical experiments of the flow around a $10M_\oplus$ core. One series of simulations vary the character of the background flow, by varying the components of gravity due to the disk that are included in describing the flow and by varying the background power laws of density and temperature. A second series of simulations vary the thermodynamic treatment of the gas, by changing the equation of state assumed for the gas and by changing the absolute scale of the background temperature. In table 1 we summarize several important parameters of the simulations.

Columns 1-3 in the table specify a distinct label for each simulation and its resolution both in terms of the physical extent of the simulation cube, the number of grid zones and depth of the nesting. Columns 4-7 define the power law exponents, p and q, for the surface density and temperature used to define the initial conditions of the global disk system, the assumed background temperature and a reference to the assumed equation of state for each model. Columns 8-10 specify whether or not gravitational forces arising from the disk components described in sections 2.2.1 and 2.2.2 have been included in the interactions with each other and the planet core in each simulation. The last column is the duration of each simulation in years.

In the discussion below, we will first describe the evolution of a 'prototype' model *tm20*, that is typical of the results obtained in many of our simulations. Then we will describe the results of our experiments that varied the rotation curve of the underlying disk, followed by experiments that varied the equation of state and background temperature of the disk.

3.1 Morphological evolution of our prototype model

In the discussion that follows and throughout this paper, we designate the model labeled *tm20* as our 'prototype' model. Its features are typical of most of our simulations and the physical model underlying it is the most inclusive. This model was run with an ideal gas equation of state, with $\gamma = 1.4$ and included gravity from both the star and the core, as well as from both the global and local disk material.

In figures 2–5, we show 2D slices of the simulation volume, taken through the disk midplane at a time 74 yr after the beginning of the simulation. In successive figures, we show the gas density, its entropy as defined by the expression

$$\log S = \log\left(\frac{p}{\rho^\gamma}\right), \tag{22}$$

its temperature and its velocity vectors projected onto the disk midplane.

The density structures are highly inhomogeneous and become progressively more so closer to the core. Densities both above and below that of the background flow exist due to the development of hot 'bubbles' in the flow near the core, which then expand outwards. One such bubble is particularly visible in the plots of the temperature distribution, emerging to the lower right. Such structures are common over the entire the duration of the simulation and emerge in all directions, depending on details of the flow at each time. Those details vary with time because of the very strong feedback cycle that is generated as outgoing bubbles perturb the incoming gas flow that is responsible for generating later activity. Activity persists for as long as we have simulated the evolution without significant decay or growth. Also, although we have not included figures illustrating so explicitly, we note that plots of slices through our simulations in directions perpendicular to the midplane show similar features: density structures which are highly inhomogenous, which become progressively more so closer to the core.

Several ring-like structures surrounding the core are visible and are remnants of intermittent large scale mass outflows ('eruptions') from the environment of the core. These rings are sheared into an ovoid shape in the disk midplane, but are near spherical in the radial plane. The eruptions themselves appear at least in part to be the result of hot bubbles that develop, expand and escape into the background flow and are due to shocks and compressional heating very close to the core.

The structures within 1–$2R_\mathrm{A}$ of the core show little evidence of spiral arms seen in some previous work (e.g. Lubow *et al.* 1999; D'Angelo *et al.* 2003b), but evidence for the development of other irregular dynamical structures is ubiquitous. Material orbiting the core or falling towards it encounters other material on different trajectories, generates shocks and heats the gas, causing bubbles and other complex morphological structures to develop. In actuality, such 'orbits' are more often little more than single passes past the core as mass from the surrounding disk first falls into the core's gravitational influence, then returns to the disk and is swept away.

We attribute the origin of the bubbles to the combination of four conditions of our simulations. First, we include only a very small gravitational softening coefficient for the core, which means that the depth of its gravitational potential well is very deep and that the energy available for conversion into heat is very large. Second, we include no explicit viscosity in our formulation of the fluid equations, so that features of the flow are not blurred or otherwise damped out by dissipative effects beyond our ability to model with precision. Also, our numerical method exhibits both very low numerical dissipation and very high fidelity for capturing the physical dissipation due to shocks that develop in the flow. Third, we do not include any mechanisms for energy to be lost from the gas once it is converted to thermal energy from gravitational potential energy. The most important such mechanism is of course, the losses that occur as the gas cools through radiation of photons. Finally, we do not include any mechanism for accreting material onto the core, because the dimensions of our finest numerical grid are comparable to the actual radius of the core. The thermal energy carried by that material is therefore also not accreted, remaining instead with the gas. In combination, these factors ensure thermal energy is produced efficiently, as flow features remain distinct enough to resolve the strong shocks that develop during the passage of material through

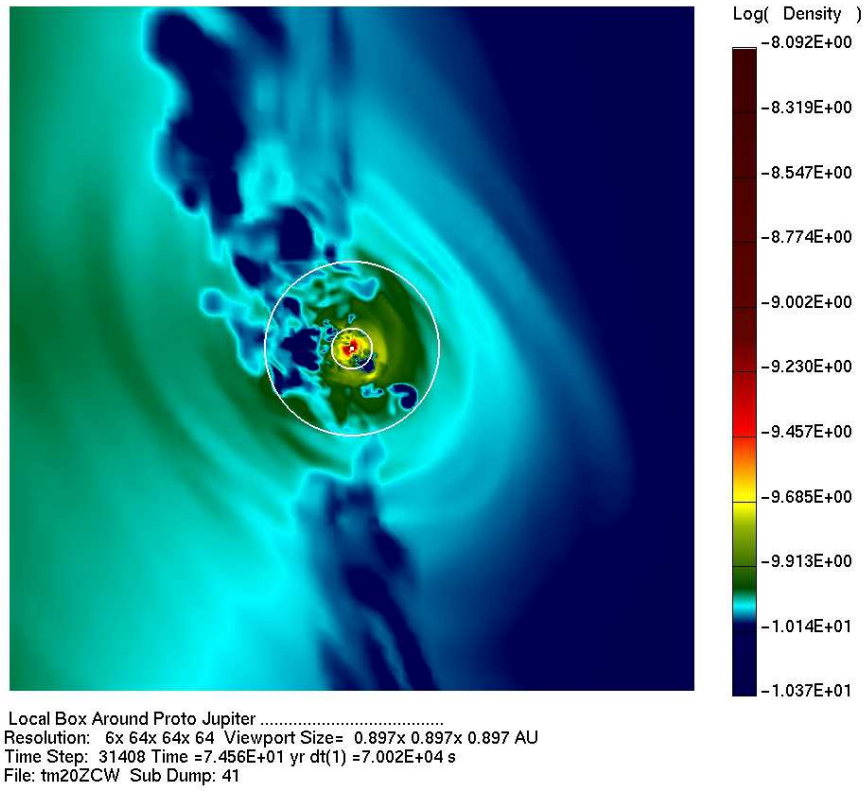

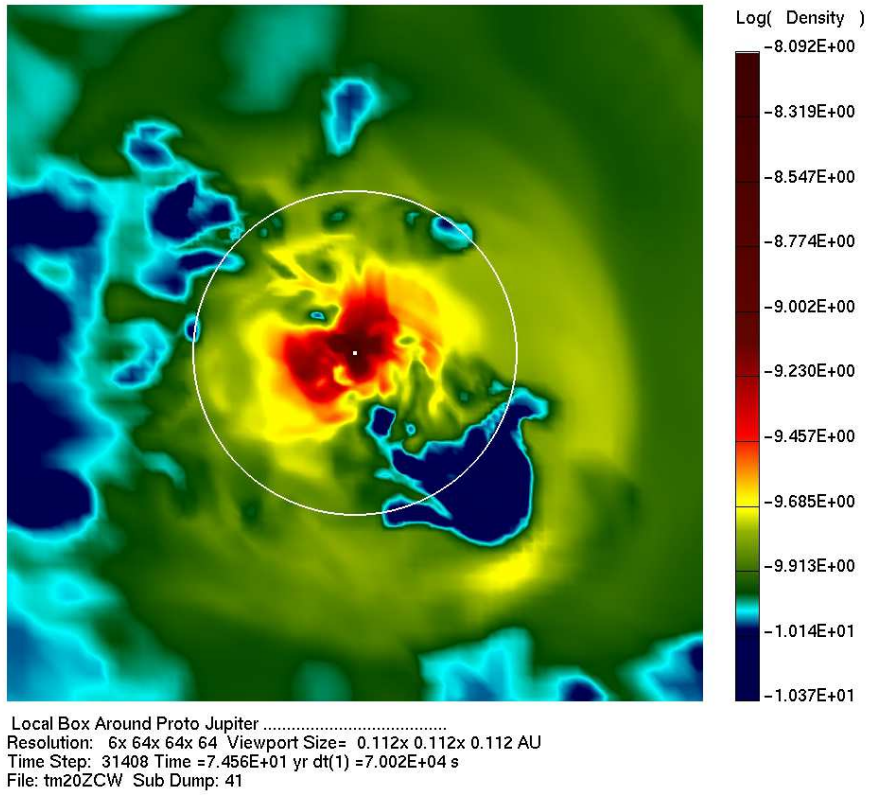

Figure 2. The volume density in a 2D slice taken through the disk midplane for the full simulation volume of $\pm 4 R_{\rm H}$ (top), and a blowup of the region within $\pm 1/2 R_{\rm H}$ of the core (bottom) The spatial extent of each frame, in AU, is defined in its caption and labeled "Grid Size". Each cutout intersects the planet core at the origin. The white circles define the radius of the accretion sphere $R_A = GM_{\rm pl}/c_s^2$ (small circle) and the Hill radius (large circle). The color scale is logarithmic and extends from $\sim 10^{-10}$ to $\sim 10^{-8}$ g cm^{-3}.

Table 1. Simulation Parameters

Label	Resolution	Simulation Box Size	p	q	$T_{\rm pl}$	EOS	Global Disk on Planet	Global Disk on Local Disk	Local Disk on Local Disk	T_{end}
lo10	3×64^3	$\pm 4 R_{\rm H}$	1.0	1.0	200 K	eq. 8	no	no	no	1600 yr
ft10	5×64^3	$\pm 4 R_{\rm H}$	0.5	0.5	200 K	eq. 8	no	no	no	100 yr
fl10	5×64^3	$\pm 4 R_{\rm H}$	0.5	1.0	200 K	eq. 8	no	no	no	100 yr
br10	5×64^3	$\pm 4 R_{\rm H}$	1.0	1.0	200 K	eq. 8	no	no	no	100 yr
bp10	5×64^3	$\pm 4 R_{\rm H}$	1.0	1.0	200 K	eq. 8	yes	no	no	100 yr
bs10	5×64^3	$\pm 4 R_{\rm H}$	1.0	1.0	200 K	eq. 8	yes	yes	no	100 yr
sg10	5×64^3	$\pm 4 R_{\rm H}$	1.0	1.0	200 K	eq. 8	yes	yes	yes	100 yr
so10	5×64^3	$\pm 4 R_{\rm H}$	1.0	1.0	200 K	eq. 8	yes	yes	no	100 yr
sg20	5×64^3	$\pm 4 R_{\rm H}$	1.0	1.0	200 K	eq. 8	yes	yes	yes	100 yr
b05h	6×64^3	$\pm 6 R_{\rm H}$	1.0	1.0	50 K	eq. 8	yes	yes	no	100 yr
tm05	6×64^3	$\pm 6 R_{\rm H}$	1.0	1.0	50 K	eq. 8	yes	yes	yes	100 yr
tm10	6×64^3	$\pm 5 R_{\rm H}$	1.0	1.0	100 K	eq. 8	yes	yes	yes	100 yr
tm20	6×64^3	$\pm 4 R_{\rm H}$	1.0	1.0	200 K	eq. 8	yes	yes	yes	100 yr
tm40	6×64^3	$\pm 4 R_{\rm H}$	1.0	1.0	400 K	eq. 8	yes	yes	yes	100 yr
iso1	6×64^3	$\pm 4 R_{\rm H}$	1.0	1.0	200 K	eq. 11	yes	yes	yes	100 yr
iso2	6×64^3	$\pm 4 R_{\rm H}$	1.0	1.0	100 K	eq. 11	yes	yes	yes	15 yr
iso3	6×64^3	$\pm 4 R_{\rm H}$	1.0	1.0	50 K	eq. 11	yes	yes	yes	15 yr
adi1	6×64^3	$\pm 4 R_{\rm H}$	1.0	1.0	200 K	eq. 12	yes	yes	yes	150 yr

the core's environment, and dissipated (or simply lost, as in the case of accretion onto the core) inefficiently since no mechanisms are included to do so. Instead, the thermal energy is converted again into kinetic energy as the high pressure gas expands outwards in bubbles and rejoins the background flow. We will explore the consequences of energy loss mechanisms in section 4.4 below.

Variations in entropy are significant in our simulations because the physical model includes only one mechanism by which its value can change after a packet of gas enters the simulation volume. Specifically, the hydrodynamic scheme itself generates entropy at shocks as a consequence of nonlinearities in the solution of the fluid mechanics equations there. Therefore, any increase in entropy is, by assumption, a very strong *a posteriori* indication that shocks developed in the flow. Other entropy generation mechanisms that might be present in the flow will exhibit different characteristics than we observe in our simulations. For example, entropy generation in turbulent flows would be characterized by a conservative cascade of energy flow from large to small scale flow features, followed by entropy and thermal energy generation at small scales. Such a cascade is not observed, and we believe turbulence is not an important characteristic of the flow activity present in our simulations.

The fluid entropy in the background flow shows essentially no visible variation at different locations in the flow. Entropy of material near the core increases as it undergoes irreversible heating in shocks, but such heating is highly inhomogeneous and low entropy material is frequently present at distances only a small fraction of the accretion radius from the core itself. For example, comparing the bottom, high resolution, panels of figures 3 and 5 (discussed below), we see that low entropy 'background' material (i.e. the dark blue shaded material in figure 3) in the upper right quadrant of the images is falling rapidly towards the core. Despite its proximity, it remains as essentially pristine background disk material until it falls to a distance of only $\lesssim 0.1 R_{\rm A}$ (or equivalently, a few times Jupiter's current radius, R_J) from the core. There, its motion is strongly perturbed by the gravitational forces it experiences, which alter its trajectory onto paths that intersect those of other nearby packets of matter, generating shocks. As it re-enters the background flow, high entropy material begins to mix with the un-shocked background material, but the mixed material remains distinct from the background until it leaves the simulation volume.

Figure 4 shows the material temperatures for the same snapshots as seen in figure 2. Temperatures as high as 6000 K are common in the innermost envelope, within distances of $\sim 0.1 R_{\rm A}$(or as we note above, a few times Jupiter's current radius, R_J), but quickly drop to a few hundred degrees at larger separations. Most material at and outside the accretion radius, $R_{\rm A}$, is only slightly warmer than the background 200 K flow. Exceptions are materials that are clearly remnants of dynamical activity nearer to the core which expand outwards, such as the large mushroom shaped feature extending to the lower right in the figure. Apart from the radial temperature variation assumed for the background flow, visible temperature fluctuations of large magnitude do not extend away from the core to nearly the distances that are seen for the density variations. Nevertheless, material that has undergone a close encounter with the core does remain warmer and can be distinguished from the background flow even as it leaves the simulation volume, some time after the interaction occurred.

It is of some interest to compare the distributions of temperature and entropy near the core. Although large deviations are present, the temperature distribution appears far more spherically symmetric than does the entropy distribution. This is important because it indicates that material may undergo adiabatic compression without being shocked while falling inwards towards the core, and only suffer a shock deep in the envelope where the activity is most dynamic. Implications of such compression and shock behavior will be discussed in section 5.

Figure 5 shows velocity vectors of the flow in the midplane at the same time as is shown in figure 2 above. In conflict to the orbital predictions from pure celestial mechanics that the flow of material approaching the Hill volume will

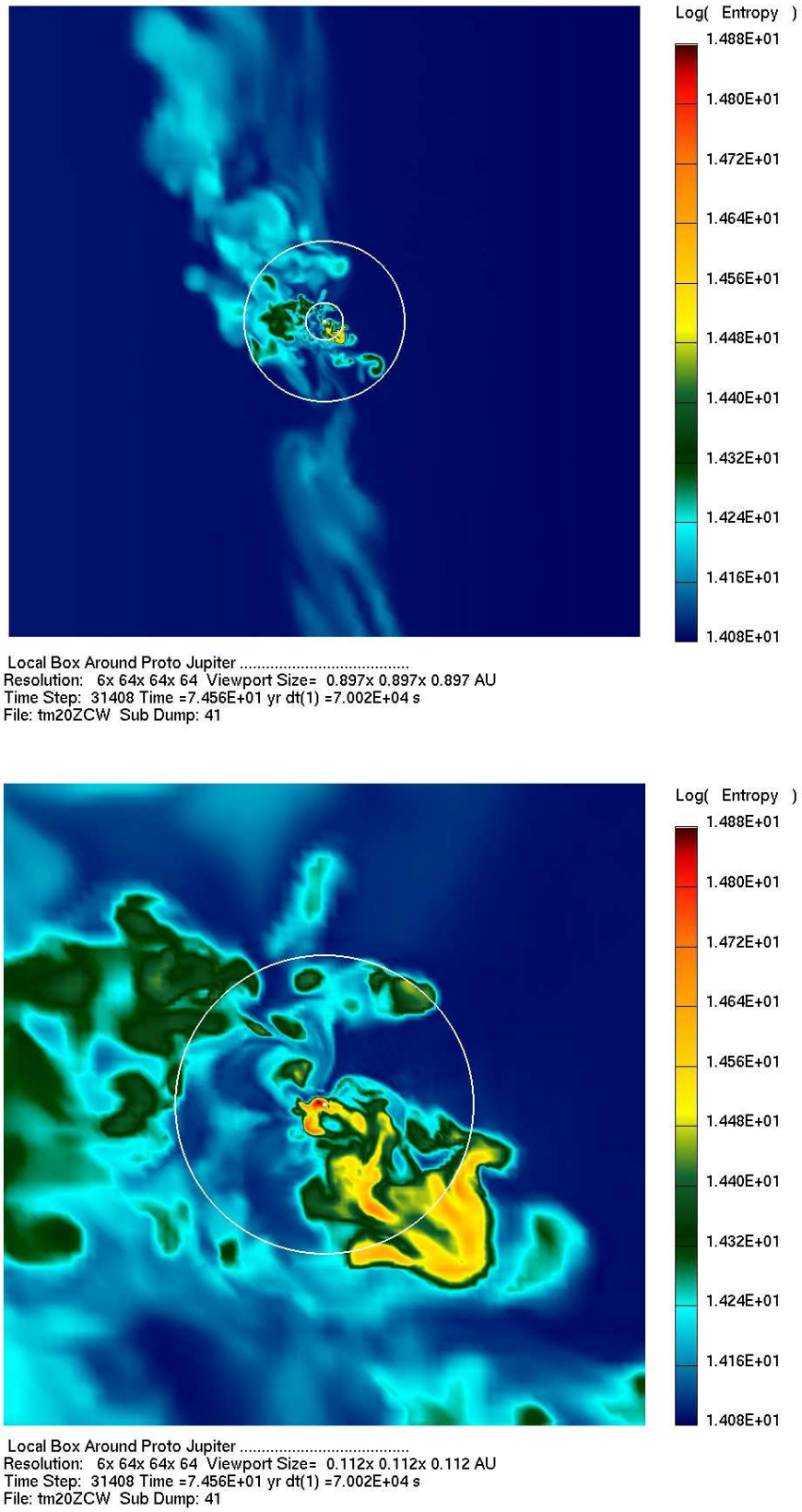

Figure 3. As in Figure 2, but showing entropy. The background flow is characterized by a small radial entropy gradient. Entropy increases by a factor ~ 6 over this value in the highly shocked neighborhood of the core, then decreases, as it mixes in with the low entropy background material in post-encounter evolution.

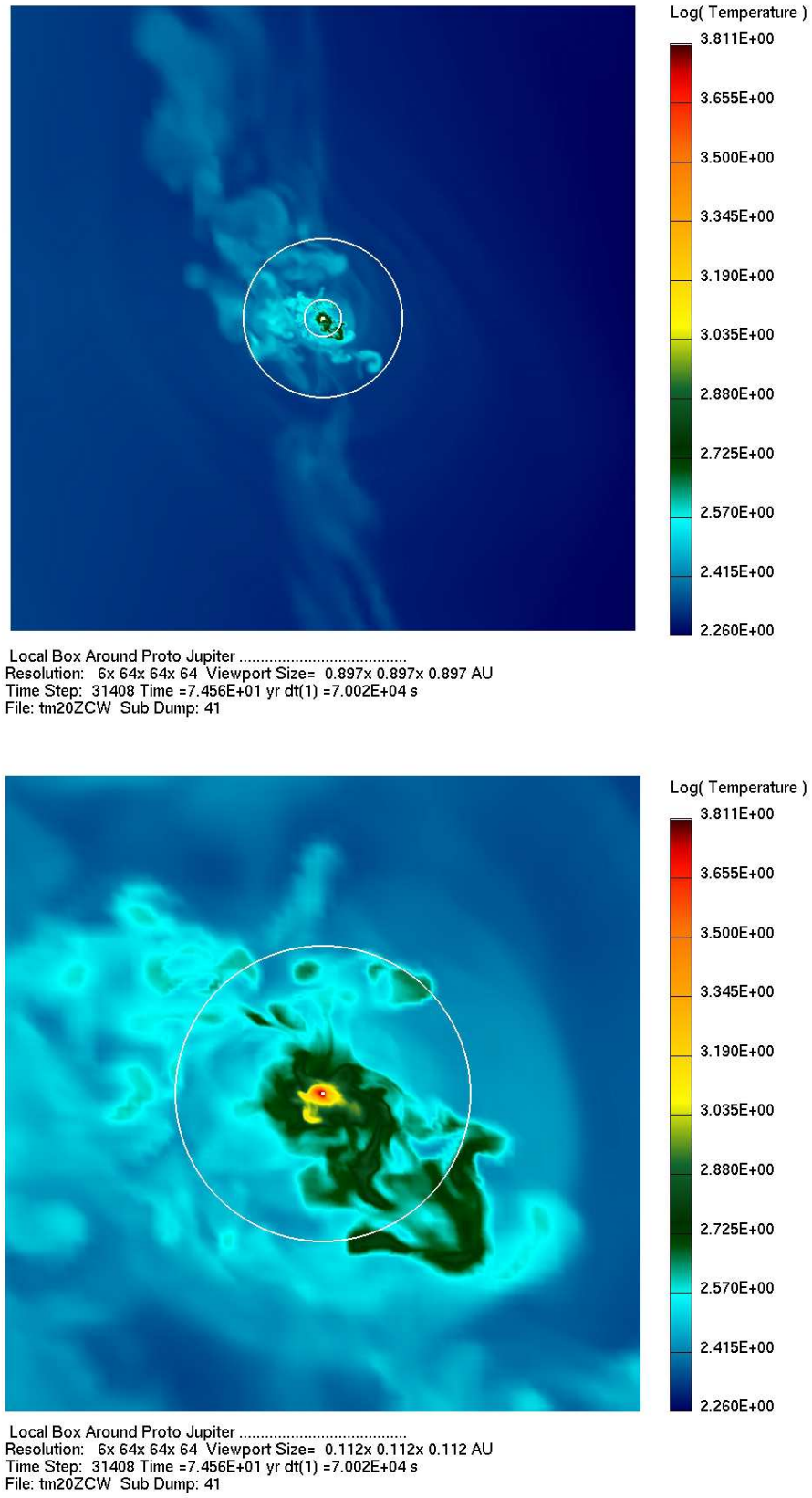

Figure 4. As in Figure 2, but showing temperature. The color scale is logarithmic and extends from 180 to 6500 K. Temperatures as high as 3-5000 K are common very close to the core, with temperatures decreasing rapidly to the background $\sim$ 200 K value at increasing distance.

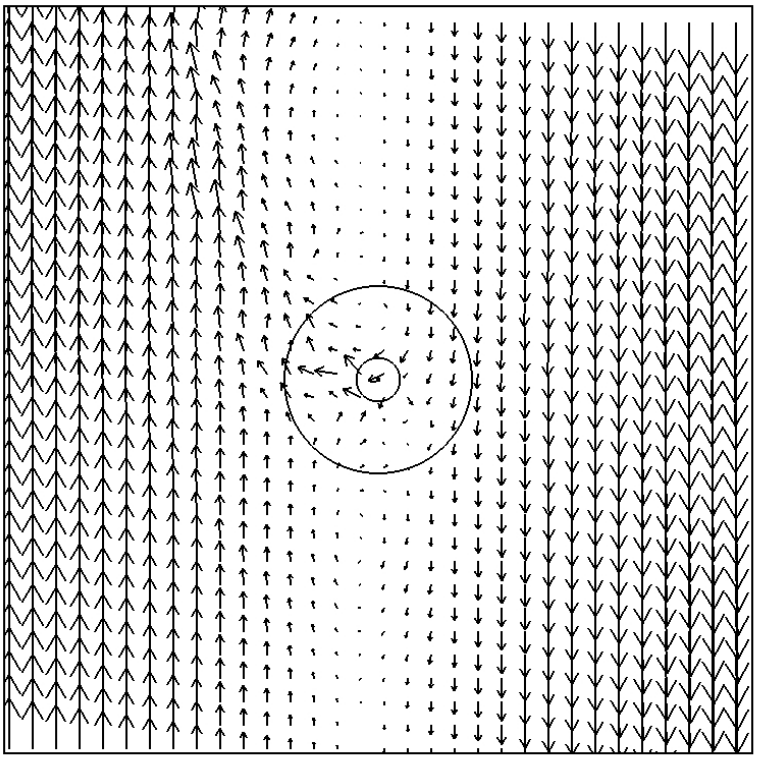

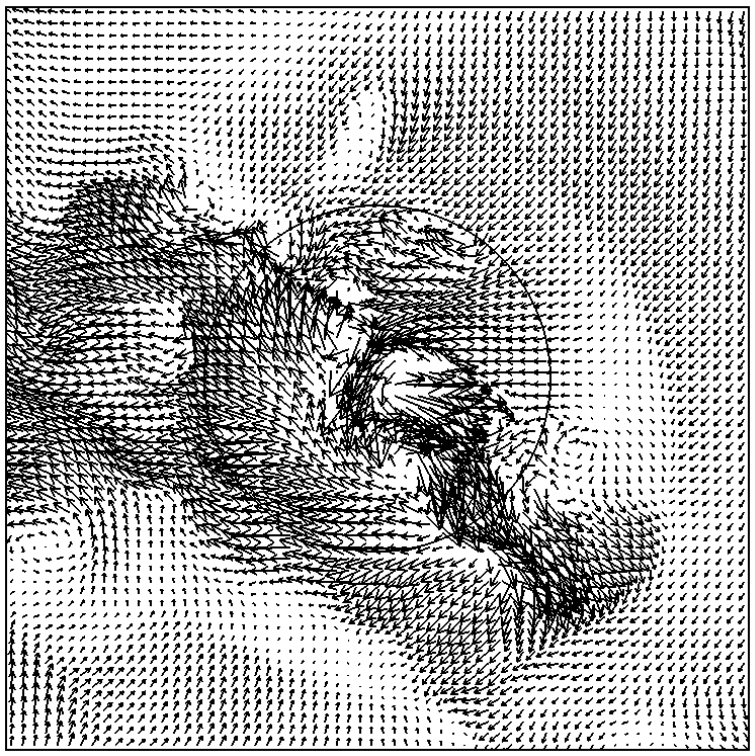

Figure 5. Velocity vectors shown projected onto the disk midplane on the coarsest grid in the top panel, and on the fourth nested grid in the bottom panel.

turn around on a 'horseshoe' orbit, matter approaching the outer portion of the Hill volume can be nearly unaffected, often passing completely through its outer extent with only a small deflection. At the time of this snapshot, the trajectory of material radially outward of the planet passes directly through the Hill volume nearly unaffected, while material radially inwards experiences larger trajectory perturbations even at distances well beyond the Hill radius. Although we do not include specific examples as figures here, we note that as the flow evolves over time, this pattern frequently reverses itself, exhibiting exactly the opposite behavior–material inward of the planet is perturbed only slightly, while material outwards is significantly affected to a distances of 2-3$R_{\rm H}$. We will quantify these variations in more detail in section 3.2.3, below.

In contrast with this intermittently active flow further away, material is always very strongly perturbed on the scale of the accretion radius, where large amplitude space and time varying activity develops. This too conflicts with the orbital mechanics picture, in which matter inside the Hill volume simply orbits the core. Pristine disk material can enter the Hill volume from the background flow and shocked, high entropy material can escape and rejoin the background flow. Changes in the flow pattern occur on time scales ranging from hours to years, with a typical encounter time inside the accretion radius of less than a month. Additional discussion of these variations is found in section 3.2.3 below.

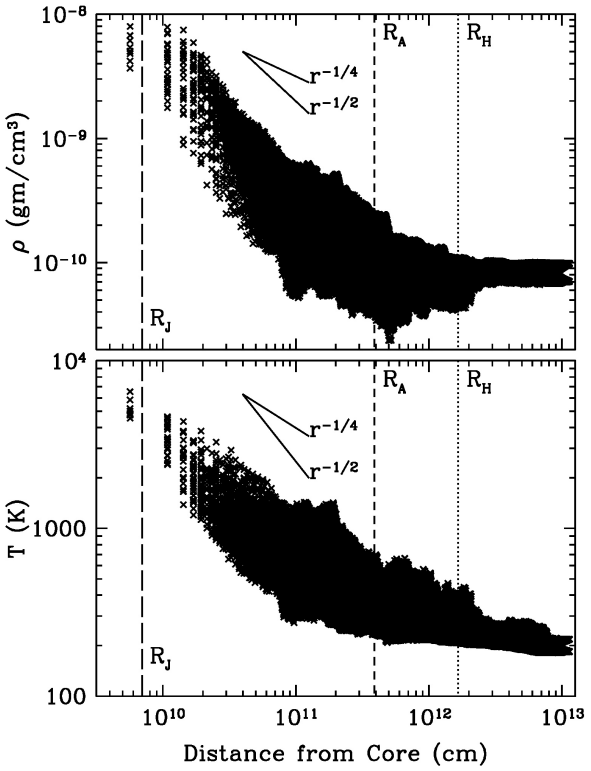

Figure 6. The volume density (top) and temperature (bottom) of the gas in our prototype model, plotted for each zone in the grid as a function of distance from the core, at time $t = 74$ yr after the beginning of the simulation. The vertical dotted and short dashed lines define the location of $R_{\rm H}$ and $R_{\rm A}$, respectively, and the long dashed line defines the present day radius of Jupiter, and is included to provide scale. Solid lines define the slopes of $r^{-1/2}$ and $r^{-1/4}$ power laws.

3.2 Quantitative metrics of the activity

The figures and discussion in the last section demonstrate the fact that the environment around the core is dynamically active in a qualitative sense, but do not quantify any measure of that dynamical activity apart from its overall morphology. Here we attempt to characterize the activity using a more quantitative analysis. First, we discuss the distributions of mass and temperature in the envelope as a function of distance from the core, then, as integrated totals of mass and angular momentum contained in the envelope at a given time. We will use two metrics to describe the latter two quantities. Specifically, we tabulate the total mass enclosed by a sphere of given radius and the total angular momentum of that material, calculated using the core as the origin of coordinates.

3.2.1 The distribution of the gas near the core, and its temperature

Because of the extremely non-homogeneous morphology and dynamically active flow, little purpose is served by attempts to reduce the flow variables to spherically averaged quantities. Nevertheless it remains interesting to analyze the overall distribution and limits of various quantities as they change as a function of radius. Such analyses are useful both to illustrate differences from the flow in our simulations from 1D models and, secondly, to quantify the extreme values that may be expected at each radius and their significance in the context of the overall evolution of the system.

Figure 6 shows the density and temperature of each grid zone in our prototype model, each as a function of distance from the core. In both cases, the distributions are nearly flat at large distances (i.e. $>>R_{\rm H}$), varying only slightly at a given distance as a consequence of the overall radial gradients of density and temperature defining the background flow in the global disk model. A quantity of material at large distances from the core exists that is clearly distinct from the background, as a population of points with somewhat higher temperatures, but is not visible in the density plot. This signature is due to material which has been processed through the core's envelope and returned to the background flow, but which has not yet fully cooled or mixed with it. The material retains its higher temperatures until it is carried out of the grid volume. An example of such flow is illustrated in figures 2-4, where a hot outflow is shown emerging to the lower right in the lower panels of the figures.

At distances smaller than the Hill radius, both density and temperature begin to deviate more significantly from their background values. At a given distance from the core, the maxima found in either quantity approach factors of $\sim 5-8$ larger than the minima at the same distance, with the largest differences occurring inside the accretion radius. Densities both increase above their background values and decrease to well below the background, reflecting both the compression of infalling material and the expansion of hot material after it is processed deep in the core's gravitational

potential well. Both quantities increase all the way to the inner radial limit imposed by our grid resolution, at a distance from the core of $\sim 5.6 \times 10^9$ cm, which is somewhat smaller than the present day radius of Jupiter itself. For the innermost zones, densities reach values of $\sim 10^{-8}$ g/cm^3, nearly two orders of magnitude above that in the background flow, while temperatures rise to 5-7000 K. Examination of lower resolution variants of this simulation (i.e. simulations *sg10* and *lo10*, not shown here), show lower maximum densities and temperatures, indicating that the values reached in figure 6 are not converged, and suggesting that still higher values might be reached near the core/envelope interface if resolution were to be increased.

Both distributions vary widely at any given radial distance from the core, and neither can reasonably be fit to a 1D power law. In particular, the density distribution cannot be fit to a r^{-2} power law, as would be expected from a spherically symmetric infall. Instead, and to the extent that it follows a single profile at all, it falls nearer to a profile between $r^{-1/4}$ and $r^{-1/2}$, as indicated by the lines accompanying the figure. The much shallower radial dependence presumably reflects the fact that no mass accretion onto the core is permitted, so that material entering the envelope is opposed by material already there, and by material returning to the disk.

The lower limits of the temperature distribution at each radius provide an interesting flow metric because they define the population of material at each radius which has undergone the least heating, either due to compression or to shocks. Of great interest is that material at temperatures below ~ 300 K is not uncommon even at distance as small as 10^{11} cm, about 1/4 of the accretion radius, while at other locations at the same distance, temperatures as high as 1-2000 K are present. The presence of low temperature material close to the core demonstrates that some fraction of the background disk material can penetrate deeply into the envelope while undergoing essentially no processing by it, either due to shocks or to adiabatic compression. This material is interesting because as it continues its trajectory through the envelope, it may subsequently undergo some compressional or shock event which heats it rapidly to temperatures more typical of other material at these distances. A quantification of what fraction of material undergoes such rapid heating, as opposed to that undergoing some slower heating process or to that simply being advected out of the envelope again, is beyond the scope of this study. Its existence is important to note however, because if an appreciable quantity of material can penetrate deeply into the envelope while remaining cold, then be rapidly heated and ejected again into the background flow, some signature of the processing may remain in material available for study today. We discuss a preliminary study of such a possibility in section 5.

3.2.2 The mass contained in the envelope as a function of time

Figure 7 shows the mass enclosed by spheres of radii, $R_{\rm A}$ and $r = 0.10$ AU$\sim 0.9R_{\rm H}$, each as functions of time. Except for the first ten year period of the simulation (omitted in the plots), in which we artificially grow the core to its final mass, the enclosed masses exhibit no secular mass accretion over

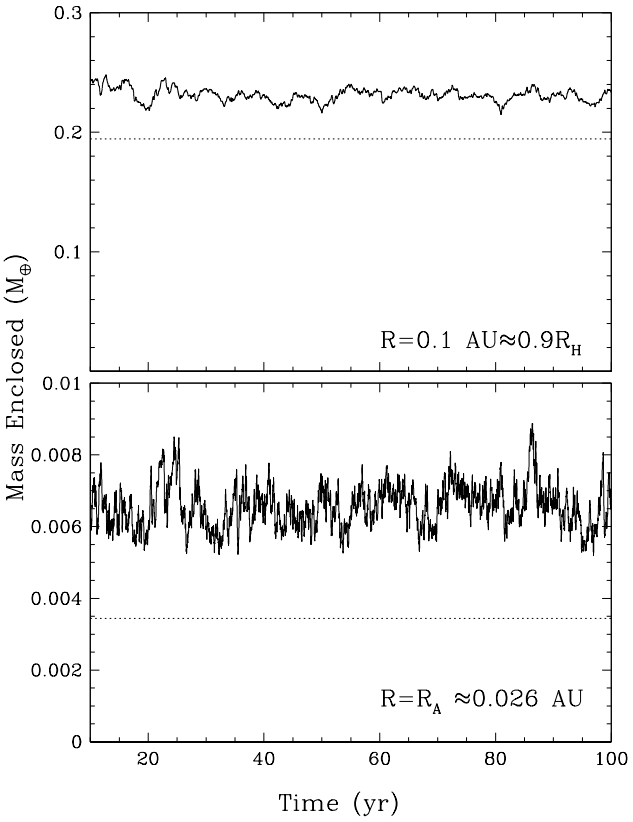

Figure 7. The mass enclosed by spheres of radius $r = 0.10$ AU$\approx 0.9R_{\rm H}$ (top) and $r = R_{\rm A} (= 0.026$ AU) (bottom), each as functions of time during the simulation. The first 10 years of the evolution define the period when we first 'grow' the core from $1M_\oplus$ to its final mass of $10M_\oplus$, thus the envelope masses at this time are not meaningful and are not included in the figure. The dotted lines correspond to the enclosed mass at $t = 0$, as characterized by the unperturbed disk background condition.

the duration of the simulation, consistent with our neglect of cooling. The amount of mass enclosed within the accretion radius is quite small, averaging $\sim .007M_\oplus$, while on the scale of the Hill radius, a quantity of $\sim 0.24M_\oplus$ collects near the planet. In comparison to the 'background flow' initial condition, the inner envelope mass has increased by a factor ~ 1.8, while the envelope mass as a whole has increased by a factor ~ 1.2.

Variations in the enclosed masses with time are visible in both curves, with magnitude $\sim 10 - 20\%$ for the smaller sphere and $\sim 5 - 10\%$ for the larger. In neither case does the variation grow or shrink as a function of time, again consistent with our neglect of cooling. The temporal character of the variability, such that any sort of periodicity can be defined at all, clearly favors higher frequency oscillations close to the core and slower oscillations farther from it. Variations on time scales well under a year are common for the accretion sphere volume, and are often superimposed on longer time scale features, as the overall morphology of the flow reacts to changes in the larger scale flow. The existence of the variations over time is a consequence of the dynamical activity discussed above, as morphological features flow into or out of the respective spheres defining our metrics. In turn,

their time scales are consequences of the shorter dynamical times deeper in the core's gravitational potential well, as compared to those farther from the core.

3.2.3 The angular momentum of the gas around the core

In addition to the mass and temperature distributions discussed in the last sections, the distribution of angular momentum of the material in the environment of the core can also provide insights into the character of activity. Here, we describe the magnitude and the variability in angular momentum distributions of material around the core. In the figures below and the discussions accompanying them, we will show both instantaneous values as functions of time, and time averages and RMS deviations over the duration of each simulation. The time dependent plots will provide insights into any periodicities that are present in the results. Time averaged quantities will be useful for comparisons between simulations with different physical parameters, and in comparison to the present day values for Jupiter. To enable such comparisons, we will present values normalized by envelope mass, as specific angular momenta.

In the discussion below, we refer to the envelope's angular momentum as its 'spin'. We caution the reader however, that this term is not strictly correct, since while some material may be in a bound orbit around the core, other parts of the 'envelope' for which spin is tabulated, may instead be more accurately classified as part of the background flow. Also, as an aid to reader's intuitive grasp of the meaning of each of the three spin components, we note that the z component corresponds to the 'top'-like motion of the planet, and corresponds to the largest component of the present day spin of the planets in our solar system (excluding Uranus). The x component defines a spin axis outwardly directed along the line connecting the star and the core and the y component defines a spin axis pointing forwards along the direction of motion of the core in its orbit.

In figure 8 we show the enclosed spin angular momentum of gas relative to the core as a function of time, in each of the three coordinate directions, and at the same two radii as the enclosed mass above. For the larger sphere, the spin magnitude oscillates, seemingly aperiodically, both above and below zero in the the x and y directions on time scales of 10-20 yr. The peaks and valleys of the oscillations extend to values as large as a few times that of Jupiter's spin, normalized by envelope mass, and typically falls in a range within ± 1 $S_{\rm J}$ of its mean. In the z coordinate, a similar feature, with oscillations of similar or slightly larger magnitude, is also present but does not cause the sign to change because the mean lies significantly below zero. The fact that the sign of the spin is uniformly negative is important because it indicates that the 'envelope' contains material which is merely passing through the Hill volume as part of the background shear flow. It is not a part of either a static or forwardly-rotating envelope, as expected in a purely dynamical flow in which pressure plays no role.

On the smaller scale of the accretion radius, where we would expect the matter flow to be influenced more by the core, the enclosed spin per unit mass again lies near parity with present day Jupiter. Its magnitude varies on time scales much smaller than a year, both above and below zero (i.e. both one direction and the other), in all three coordinate directions. The time variations for this smaller enclosing sphere do not appear to be well correlated with any of the longer variations visible in the larger sphere. In large part, this is a consequence of the much larger total mass enclosed by the latter, so that the variations on small scales are simply washed out.

Combining the results of figure 7, which shows that the envelope contains only a tiny fraction of the present day mass of Jupiter, with those of figure 8, which shows spin normalized to the envelope mass, we find that actual spin magnitudes are only a small fraction of present day Jupiter's total spin. At such an early stage in the evolution, such a value is not particularly surprising. Close examination of the spin characteristics remains interesting nonetheless, for several reasons. First, perhaps the most important feature of figure 8 is not a exact values that any spin component takes, but rather that the amplitudes of each component (apart from the background shear of the disk included in the z spin calculation), are quite similar. This indicates that the spin direction of the planet itself is not yet fixed. The era of giant impacts between nascent cores may still continue during this phase of planet formation, with little evidence remaining in the spin characteristics of the planet in its final configuration.

Secondly, the similarity between the spin magnitudes seen here and those of Jupiter indicates that no angular momentum loss mechanism must be invoked in the circumplanetary environment in order for accretion to proceed. The most common such mechanism would, of course, be a circumplanetary accretion disk through which circumstellar disk material would pass as it accretes onto the core. No such disk appears neccessary at this early stage of the planet's evolution.

Third, the envelope's spin direction does not appear to be established: it changes sign in all three coordinate directions on spatial scales comparable to $R_{\rm A}$ and it changes sign in x and y even on much larger scales. Also, although the z coordinate spin in the $r = 0.1$ AU enclosing sphere varies widely, it varies around a negative mean value. At this scale, a purely dynamical flow (i.e. that of a set of 'test particles', affected by gravitational and fictitious forces only), would be expected to produce forward envelope rotation (positive s_z) as mass continues to accrete. Instead, some portions of the background material flow through the Hill volume, because the purely dynamical picture is incomplete. The flow is not dominated solely by the gravitational forces of the core and star combined with the fictitious forces present in a rotating medium, but also by the pressure forces of the gas itself. We will discuss the relative importance of the hydrodynamic effects in more detail in section 4.4.2, below.

4 SENSITIVITY OF THE ACTIVITY TO NUMERICAL AND PHYSICAL PARAMETERS

The dynamical activity shown in the results above persists as long as we are able to run our simulations–typically about 100 years of simulation time for each run. Unfortunately, that time is quite short compared to the time scale for the envelope to grow in mass or for the disk as a whole to evolve. We are therefore unable to answer many important ques-

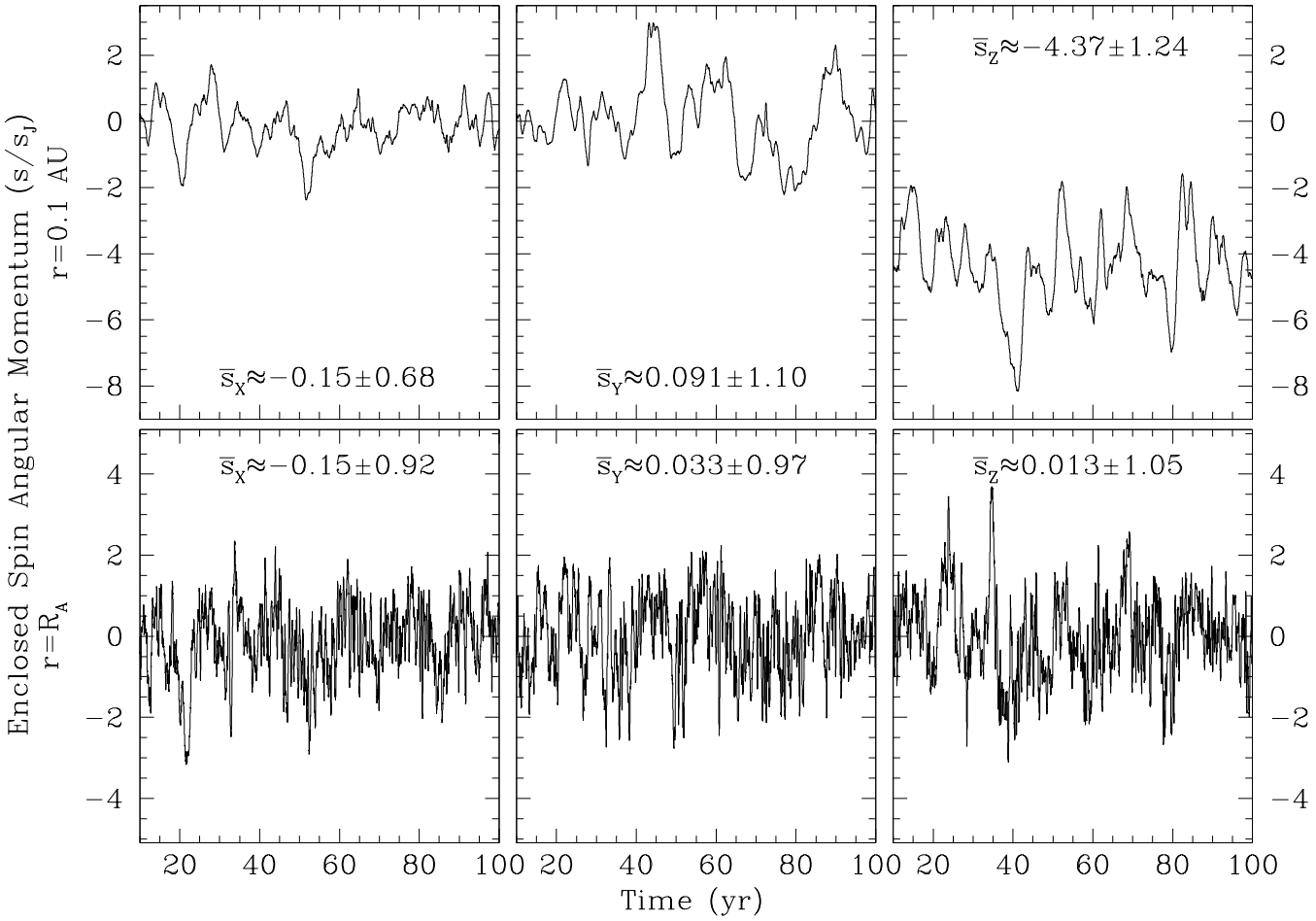

Figure 8. The spin angular momentum per unit mass calculated around the core for gas enclosed by a sphere of radius $r = 0.1$ AU($\approx 0.9R_{\rm H}$) or by a sphere one accretion radius ($r = R_{\rm A}(\approx 0.026$ AU) in size (top and bottom respectively). For the larger sphere, the net z spin has a negative bias due to the shear of the background flow. Both the x and y spins are centered near zero. All three exhibit large amplitude swings in magnitude, including changes in sign: the sense of rotation around the core reverses itself. In contrast, the spin components enclosed by the accretion radius exhibit almost no systematic trends except a continuing large amplitude and short term variation.

tions regarding the activity. In particular, in order to make broadly applicable conclusions about the physical systems we are modeling, we must show that they are common to a wide variety of initial conditions that may be encountered in the circumstellar nebula at various times in its evolution, that they are common to a variety of physical models, and that they are not unduly contaminated by consequences of our initial conditions. The results must not simply be 'start up transients' or other artifacts of initial conditions that do not represent the true system with sufficient fidelity.

To fully address these concerns requires models far more sophisticated than are presently possible and we defer discussion of any final determinations of their answers to the future. Instead, in this section we consider a number of simple parameters that can be varied within the context of our models, and to which we may reasonably suspect that our models may be sensitive. If our models vary their behavior in these, admittedly crude, sorts of parameter studies, we may justifiably conclude that they will be even more sensitive to the much more varied and variable physical properties present over the lifetime of a circumstellar disk. In addition, there may be unaccounted for numerical issues besetting our simulations which cast doubt on the results. If the simulations are comparatively insensitive to the parameters varied here, we will make a first step towards the physically meaningful conclusion that the dynamical activity discussed above can be present at interesting levels at many different times during circumstellar disk evolution.

As a useful means to quantify similar and dissimilar behavior, we adopt the spin of the envelopes, introduced in the last section, as a metric suitable for our purposes here. We summarize the time averaged quantities for each of the simulations discussed above and in the following sections, in table 2. As in table 1, the first column defines the simulation name. The next two pairs of columns (columns 2/3 and 4/5) each specify the time averaged spins and their variances of the envelope material enclosed by spheres of $r = 0.1$ AU and $r = R_{\rm A}$, respectively, for each simulation. Both quan-

Table 2. Time Averaged z components of Spins and Spin Variances

Label	s_z/s_J $r = 0.1$AU	σ_s $r = 0.1$AU	s_z/s_J $r = R_A$	σ_s $r = R_A$	CR offset δa (R_H)
lo10	-3.54	0.99	0.28	0.73	-0.219
ft10	-4.63	1.31	-0.05	1.20	-0.039
fl10	-4.40	0.91	0.005	0.97	-0.172
br10	-4.75	0.93	-0.43	1.19	-0.203
bp10	-4.83	1.31	-0.53	1.15	-0.344
bs10	-4.48	1.27	-0.13	1.19	-0.203
sg10	-4.68	0.98	-0.18	1.13	-0.203
so10	-3.99	0.07	-0.17	0.03	-0.203
sg20	-3.36	1.71	-0.03	1.93	-0.156
b05h	-2.75	1.70	0.60	1.67	-0.053
tm05	-2.26	1.50	0.78	1.54	-0.053
tm10	-4.26	1.43	0.11	1.41	-0.103
tm20	-4.37	1.24	0.038	1.05	-0.203
tm40	-5.53	0.76	-0.52	0.82	-0.39
iso1	-2.59	0.31	1.44	0.42	-0.203
iso2	-	-	-	-	-0.102
iso3	-	-	-	-	-0.051
adi1	-3.88	0.13	-0.22	0.15	-0.203

tities normalized to the angular momentum per unit mass of present day Jupiter. For the series of simulations with varying background temperature (*tm05-tm40*), the sphere of radius R_A, is replaced by one of radius $r = 0.025$ AU, for consistency, as discussed in section 4.4.2. For the *iso2* and *iso3* simulations, no time averages are reported, due to their short duration. The last column specifies the radial offset of the corotation radius from the planet that results from each physical model. We explore the importance of variations in this quantity below.

4.1 Sensitivity to the changes in the rotation curve

The dynamical activity seen above is clearly driven by interactions between the background flow and the core, mediated by hydrodynamic interactions deep in the core's gravitational potential well. We saw that the background flow could be distinguished from the local envelope to much smaller distances than are predicted by purely dynamical models. We also saw that background material could penetrate deeply into the core's potential well before undergoing substantial thermodynamic evolution such as compression or shock heating. It is therefore reasonable to ask whether features of the background flow may influence the strength of other properties of the activity. Does changing properties of the background flow change the behavior of activity generated in our simulations?

Two important properties of the background flow are first, the overall shear itself and, second, the radial location of 'corotation' relative to the orbit radius of the core itself. The first is largely a consequence of the near Keplerian orbital flow in the disk and, while other rotation curves may be of interest in some systems (e.g. galaxies), they are of no practical importance in the present context. The relative positions of the core and of the disk material orbiting at the same frequency is of much greater interest. It may shift signficantly due to the overall mass of the disk (and whether that mass is included self consistently in a calculation of the rotation curve), its temperature profile and its density profile. To what extent will such shifts affect the flow around the planet itself?

Although only a model that includes all components of gravity on all components of the system can be correct, including, excluding or otherwise modifying one term or another will allow us to explore the sensitivity of the results to that term. Here, we will include the effect of gravity and pressure in several different ways in order to explore the sensitivity of the results to the importance of the rotation curve of the disk, and the offset it may have relative to the orbit velocity of the planet. All experiments will include the gravitational force of the star and the planet as a fixed background. In separate simulations we will add additional sources of gravitational force, component by component. Parameters for each of these simulations, and the position of the co-rotation resonance relative to the core for each of these simulations are tabulated in Tables 1 and 2.

In figures 9 and 10 we show the z component of spin per unit mass enclosed inside spheres of the same two radii around the planet as are shown in figure 8, for a variety of different physical assumptions about the underlying rotation curve. In every case, variations qualitatively similar in both magnitude and time scale to those seen for our prototype model are present. Quantified in terms of their variances over time, the spins in each of the models vary by as much or more than the present day normalized spin of Jupiter over time scales much shorter than the 100 yr lifetime of our simulations. As expected from their different initial conditions, differences appear in the time averaged spin values, with a spread of about half of the present day normalized spin of Jupiter between the maximum and minimum seen in a given model. Of note is that the spread in the average values is smaller than the variations seen over time in a single model. No model stands out as particularly different from the others, nor are the results of any model particularly different from that of the prototype model discussed in section 3.1. In fact, the difference between the prototype's averages and those of the *sg10* simulation, which uses an identical physical model but one less grid, are comparable to the differences between it and any of the other models with varying physical parameters.

We conclude that different physical conditions in the disk will generate difference in the details of the envelope activity, but will not affect its presence or overall magnitude.

4.2 Sensitivity to the description of the core itself

In addition to possible sensitivities to the background flow, we might also expect dynamical activity to be sensitive to the mass of the core and to the distribution of mass close to the core, each through the gravitational forces they exert. Both can readily be probed by varying the mass of the core and its gravitational softening length. Increasing the core mass retains the shape of the potential well, but changes its depth. Increasing the softening length changes the shape of the potential well, while decreasing its depth (see eq. 14). The softening length serves as a probe of the sensitivity to the mass distribution because, in addition to its use to reduce numerical instabilities in a simulation, its presence in the otherwise perfectly inverse square, Newtonian force law

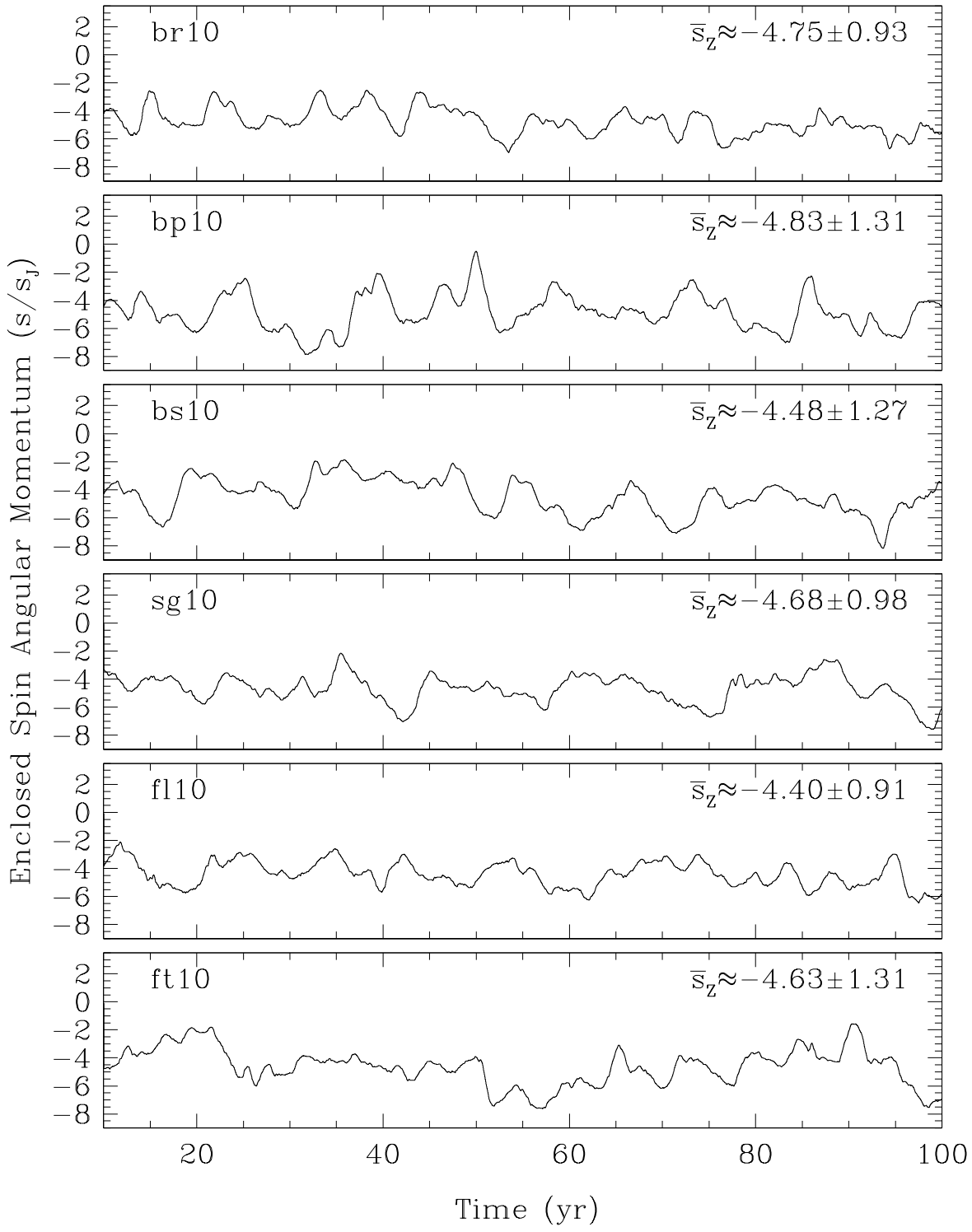

Figure 9. The z spin angular momentum per unit mass calculated around the core for gas enclosed by a sphere of radius, $r = 0.1$ AU($\approx 0.9R_H$) in size, for the model designated in the upper left corners of each panel. The time averaged magnitude of the spin and its variance are tabulated in the upper right corner of each panel.

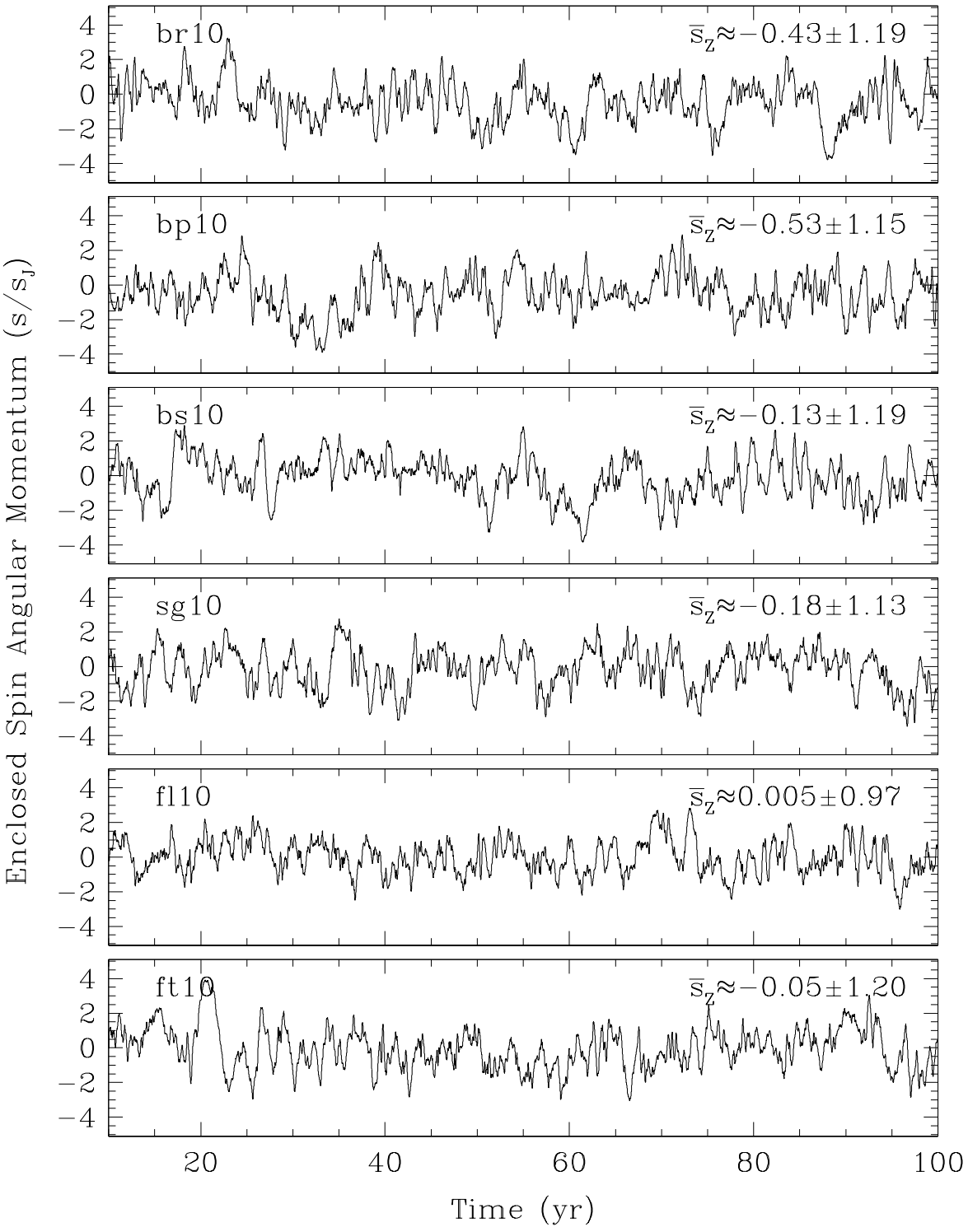

Figure 10. Same as for figure 10, but for a sphere of radius $r = R_A (\approx 0.026$ AU).

is effectively equivalent to the statement that the core's mass distribution is spatially extended on the scale of the softening length itself.

Here, we test the sensitivity of our results with two models. In one model we define a core mass of $20M_{\oplus}$, which is twice our prototype value, and in the second model, we define the gravitational softening parameter, ϵ (eq. 14), from $\epsilon = 1 \times \delta x$ to $\epsilon = 16 \times \delta x$, where δx is the size of one grid cell on the finest (in this case, the fifth) mesh. This increase corresponds to an increased spatial scale from $\sim 1.9\mathrm{R}_J$, to $\sim 30\mathrm{R}_J$, or $\sim R_{\mathrm{H}}/8$. Figure 11 shows the z spin of envelope material for these two models. In both cases, the characteristics of the envelope activity differ markedly from those of the prototype. With increased softening, the variations are near completely absent. With increased core mass, the magnitude of the variations increase by a factor of available to disk material as it traverses through the deeper gravitational potential well of the more massive core.

We conclude that characteristics of the core and envelope do affect the magnitude of the dynamical activity, and that a deep, sharp potential well is a requirement for the activity to be present. An envelope will likely exhibit dynamical activity only when the core it surrounds is sufficiently massive, and when the envelope itself is sufficiently diffuse not to contribute substantially to the shape of the potential well.

4.3 Durability of the dynamical activity

Because the duration of our simulations is short and the initial conditions are not especially tuned to begin close to any sort of equilibrium or steady state flow, it is possible that the dynamical activity is simply a consequence of inconsistencies in our initial condition. If so, then we might expect the behavior of the flow observed in a given simulation to change as a function of how long we run that simulation. In order to investigate this possibility, we have run a comparatively low resolution simulation, using the same physical model as our prototype, for more than 1600 years of simulation time.

In figure 12 we show the z spin of the envelope material as a function of time, over the life of the simulation. As for the high resolution models above, the magnitude of the spin displays continuing activity, with no signs of decrease or modulation. Inside the accretion radius, the spin direction changes on time scales of $\lesssim 1$ yr, as it does for our prototype. On the scale of the Hill volume, the overall direction (backwards relative to the present day spin of Jupiter) again retains a strong signature of the background flow, but is again perturbed significantly by the dynamical activity. In both cases, the variances around the means fall some $\sim 20\%$ smaller than were seen in the higher resolution models, but remain comparable to the normalized spin of present day Jupiter. An important difference is that a positive mean spin exists for the material inside R_{A} and, for the $r < 0.1$ AU volume, a somewhat less negative overall spin because of the opposing contributions of the inner envelope and the background flowing through the outer envelope volume.

We attribute the differences in behavior to differences in resolution because the smaller cells and time steps provided by the higher resolution realization permit more rapid and larger amplitude variations than in the lower resolution simulation. None of the differences contribute to any overall growth or decay of the dynamical activity. We therefore conclude that the dynamical activity is not due to start up transients arising from inconsistencies in our initial condition.

4.4 Sensitivity to thermodynamics

We now turn to the question of how our results depend on the thermodynamic treatment of the gas. There are two distinct physical properties that may be important for the flow. They are first the heating and cooling properties of the gas together with the equation of state and second, the temperature of the background flow. In the following two sections, we examine both of these possibilities in turn.

4.4.1 Importance of heating and cooling, as approximated by assumed equations of state

Although we do not include any external heating or cooling directly in our study, we can perform experiments comparing our ideal gas equation of state to locally isothermal and locally isentropic equations of state. Detailed discussions in Nelson *et al.* (2000) and Pickett *et al.* (2003) describe the physical interpretation of the effective heating and cooling that can be placed on simulations that use such formulations. For our purposes here, it is sufficient to note that both ordinarily imply very efficient cooling. Simulations which employ a locally isentropic equation of state effectively assume that all shock heating is instantly radiated away. Simulations which employ a locally isothermal equation of state effectively assume that all heating due both to shocks and PdV work is instantly radiated away.

Figure 13 shows the density structure obtained from locally isentropic and isothermal evolution. In each case, the morphologies are far more uniform than are seen in the evolution with an ideal gas treatment (as seen in figure 2). The density structure in the locally isentropic evolution appears nearly spherically symmetric, with only small perturbations being visible in the image, towards the upper left and lower right of the core. Over time, perturbations of similar size and magnitude appear at various positions in the envelope as the flow changes, but do not grow substantially larger.

Locally isothermal evolution leads again to fewer dynamical features in the flow than in our prototype simulation, but here some activity remains visible, predominantly in the form of a barred spiral pattern generated by material orbiting the core, along with some smaller features which are remnants of prior spiral structures that have merged or disintegrated as the evolution proceeds.

The densities in the deepest parts of the envelope in both of the simulations rise to values much higher than those seen in our prototype. The highest central densities occur in the isothermal evolution, at more than four orders of magnitude higher than in the ideal gas evolution, and two orders of magnitude higher than the isentropic evolution. The higher densities are the most visible consequences of the implied cooling assumptions in each model, which do not permit high temperatures to evolve deep in the envelope. In consequence, pressure forces opposing the gravitational attraction of the core are correspondingly reduced, which allows additional mass to concentrate there.

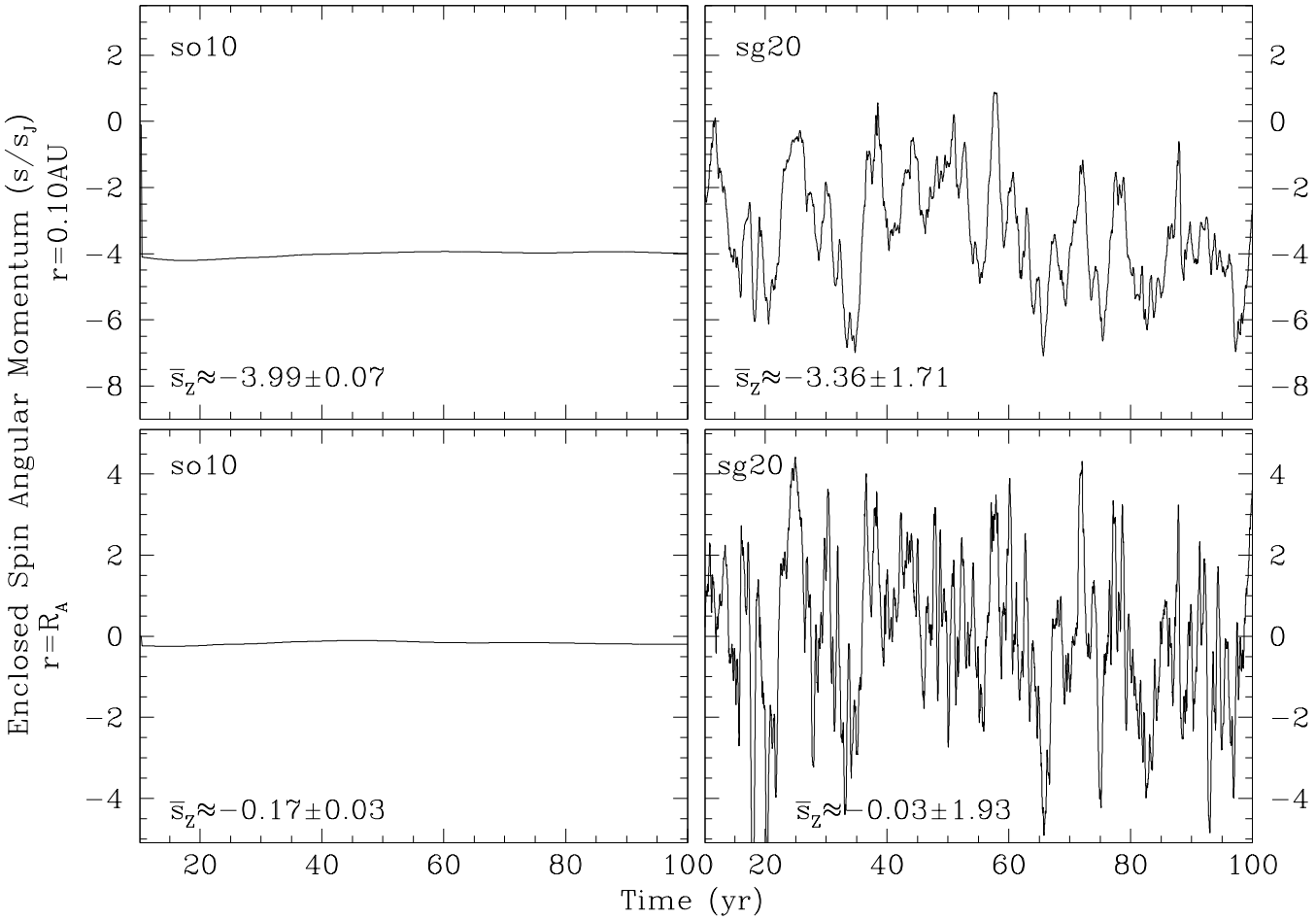

Figure 11. The z spin angular momentum per unit mass of the envelope material enclosed in spheres of radius $r = 0.1$ AU($\approx 0.9 R_{\rm H}$) (top) and of $r = R_{\rm A}$ (bottom), each as functions of time. The left panels refer to simulation *so10*, with increased gravitational softening, while the right panels refer to simulation *sg20*, with increased core mass.

We monitored the stability of the gas to numerically induced collapse through violation of the Jeans criterion (Truelove *et al.* 1997) and, although not strictly applicable to this system[1], the criterion was satisfied over the evolution of the simulation, using a safety factor of $J \sim 4$. Nevertheless, at time $t \approx 85$ yr, the gas near the core began to collapse in upon itself, and shortly thereafter we terminated the simulation. Although a strict application of the Jeans criterion is satisfied, we believe that this collapse behavior is not due to any physical cause, but rather a numerically induced consequence of the isothermal evolution and the high spatial resolution.

Figure 14 shows the evolution of the z spin of the envelope material over time, for both simulations. In both, some variability remains, particularly in the isothermally evolved model. In comparison to the variations seen in figure 8, however, the magnitudes are far smaller. Variations of only $\lesssim 0.2\ S_{\rm J}$ are found in the isentropic evolution compared to $\sim 1\ S_{\rm J}$ or more seen in figure 8. The time scales of the variations also appear somewhat longer, even for the smaller volume accretion sphere, defined by $r < R_A$, though we have made no attempt to quantify such time dependence.

Variations seen in the isothermally evolved simulation are larger than the isentropic simulation, near $\sim 0.3 - 0.4 S_{\rm J}$, but again remain smaller than those seen in the prototype. For the larger volume sphere, the spin remains consistently negative, as it does for all of our other simulations, but its magnitude is much smaller. This difference appears to be due to the fact that the spin of the inner envelope is consistently positive, acting in the opposite sense to the flow further from the core. Quantified by its behavior for $r \leq R_{\rm A}$, the sign of the envelope spin is consistently positive: though its magnitude still varies, the spin of the envelope is always oriented in the same direction as the present day Jovian planets. Positive spin orientation is an expected result for purely dynamical systems of course (i.e. those without hydrodynamic effects), because of the influence of the fictitious forces

[1] The Jeans analysis considers small, linearized perturbations of quantities away from a smooth background, while the present configuration also includes a large 'external' potential gradient, due to the core.

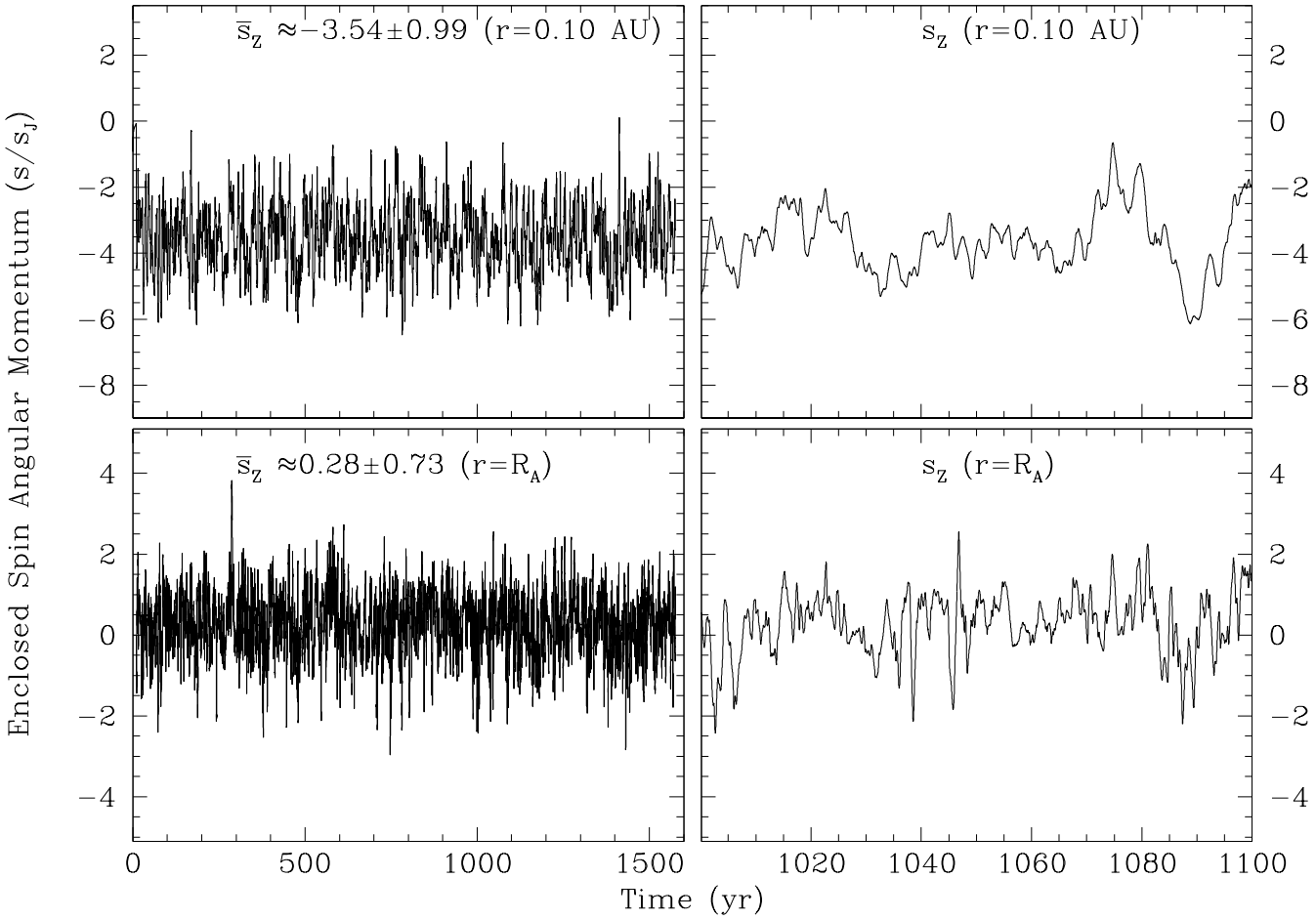

Figure 12. The z spin angular momentum of the envelope material in simulation *lo10* as a function of time, enclosed in spheres of radius $r = 0.1$ AU($\approx 0.9 R_{\rm H}$) (top) and of $r = R_{\rm A}$ (bottom). The left panels show the variation over the entire span of the simulation, while the right panels show the variation over a 100 yr segment.

on the motion. The fact that we recover a positive spin orientation *only* in this simulation, where hydrodynamic feedback is largely suppressed through the isothermal evolution assumption, provides strong support for our conclusion that the presence and strength of the dynamical activity is tied directly to hydrodynamic feedback effects on the flow. Further, it serves as an important check on the physical model underlying all of our simulations because under physical conditions where feedback is removed, the expected dynamical result is recovered.

Due to the changes in the behavior of the flow in these models, we conclude that assumptions made regarding the energy balance will be of critical importance for models of dynamical activity in the core's environment. Of these assumptions, a complete model for the radiative transport through the gas will be of primary importance deep in the envelope. A necessary corollary is that a well determined dscription of the material composition and size distribution over the range of temperatures and densities will also be critical, because of their influence on the opacities throughout the relevant envelope volume.

4.4.2 Importance of the background temperature

In section 3.2.3, we concluded that an important physical parameter in defining properties of the activity was the existence of hydrodynamic feedback in the system, arising from pressure forces. As the pressure and pressure gradients change in importance compared to other forces acting on the flow, will the character of the activity also change? Here we explore this question.

The most physically relevant parameter to vary in such a study is of course the pressure itself, or its gradient, but neither are directly accessible for use as numerical parameters in our simulations. Instead, we vary the overall background temperature assumed for the disk in different simulations. This quantity will serve as a proxy for the overall magnitude of pressure effects through the relationship defined by the equation of state. To address our question, we have run in four variants of our prototype model (simulations *tm05, tm10, tm20* and *tm40*), with background temperatures at the core's orbit radius of $T = 50$, $T = 100$, $T = 200$ and $T = 400$ K. For the $T = 50$ K model, we

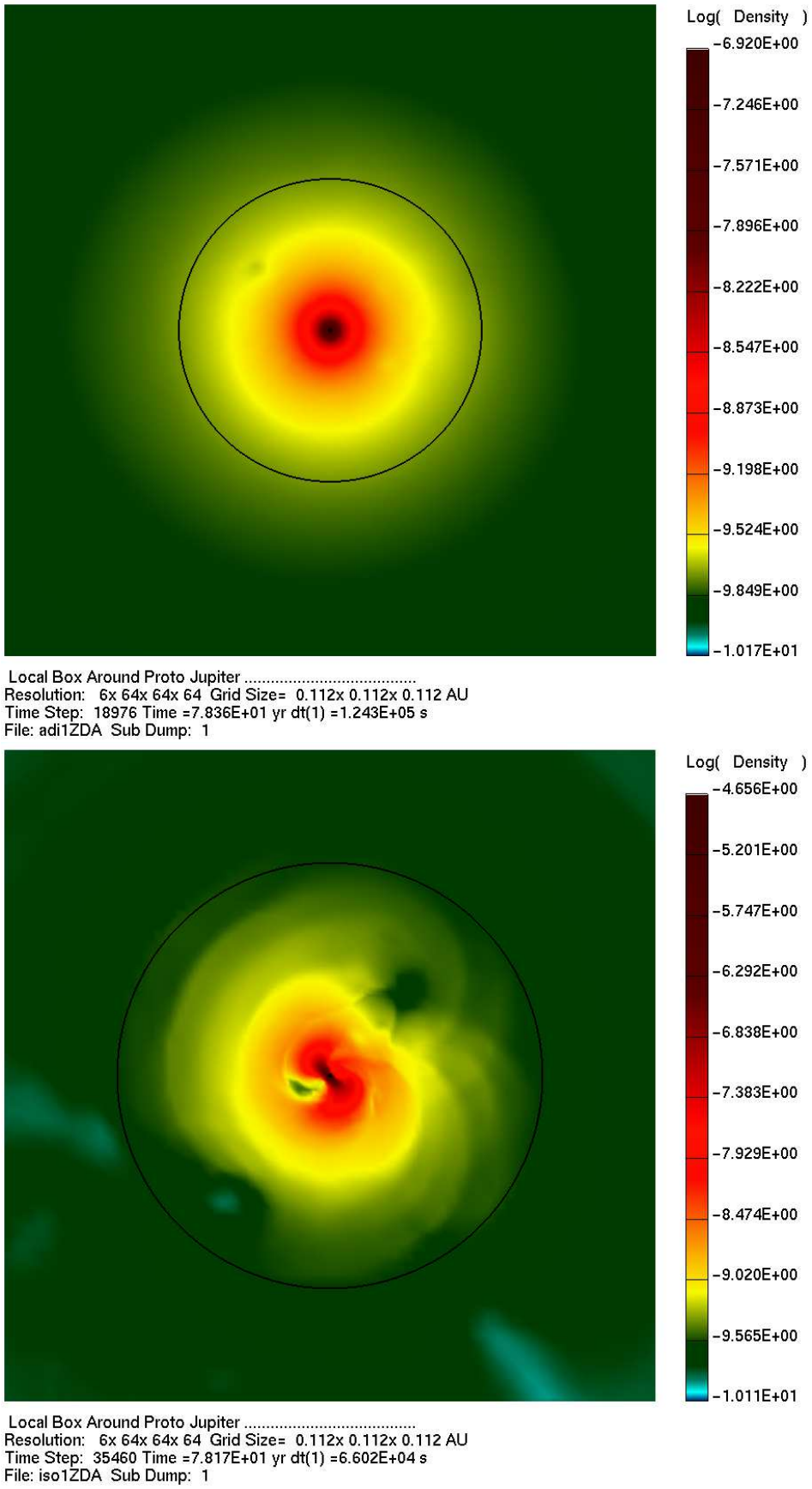

Figure 13. As in Figure 2, but showing densities for the locally isentropic (top) and isothermal (bottom) simulations. The color scales are logarithmic and extend from $\sim 7 \times 10^{-11}$ g/cm^3 in each panel to $\sim 10^{-7}$ and $\sim 2 \times 10^{-5}$ g/cm^3 for the isentropic and isothermal simulations, respectively. The black circles define the accretion radius, $R_{\rm A}$, for each simulation.

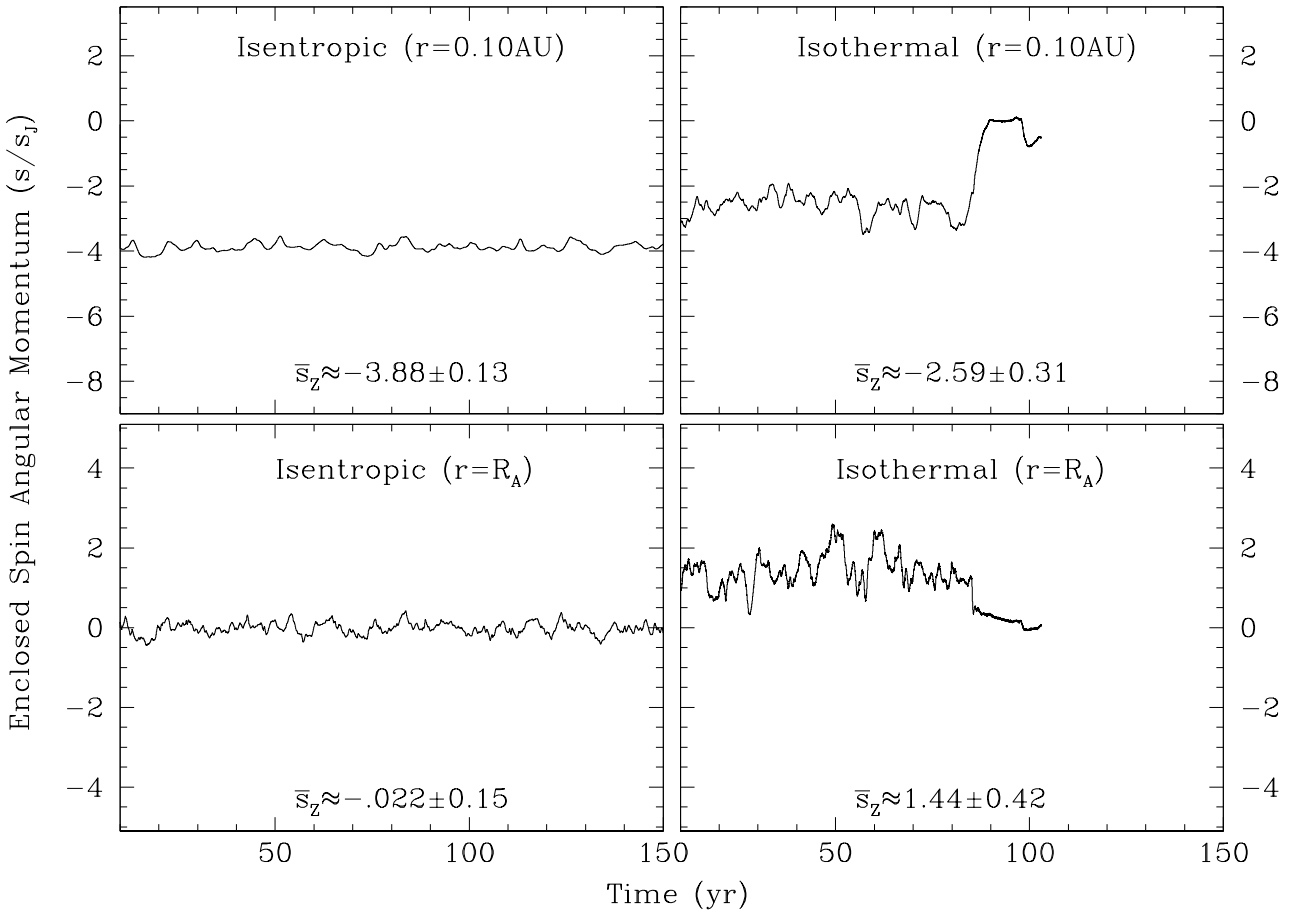

Figure 14. The z component of spin angular momentum of the envelope material, for the same two spherical volumes shown in figure 8 and for the isentropic (left panels) and isothermal (right panels) equation of state assumptions. Evolution of the isothermally evolved simulation suffered catastrophic numerical errors after $\sim$ 80 yr of evolution and was terminated (see text). Average values appearing in each panel are derived from the period spanned by [10,80] yr for the isothermally evolved simulation and [10,150] yr for the adiabatically evolved model.

also include a variant omitting local self gravity of the disk (*b05h*).

We include two variants of the model with $T = 50$ K background temperature in order to investigate the consequences of a numerical issue affecting simulation *tm05*. Due to its low background temperature and the inclusion of local self gravity, mass accumulates to an unphysical extent inside the simulation volume. We attribute this behavior to the fact that the Jeans wavelength derived for the material within the simulation volume appoximates the size of the simulation volume itself, rather than to any physical cause. Though an important consideration for other metrics, such as enclosed mass, in terms of the effects this numerical defect may have on the metric chosen in the present discussion (spin), we will find that the differences between the two simulations are minimal.

Figure 15 shows the evolution of spin of the envelope material in the z coordinate over time, for each of these simulations. From left to right, the figure shows the progression from low to high background temperatures. For consistency with the size of the sphere defined for the accretion radius in previous sections, we plot the spin enclosed by a sphere of radius $r = 0.025$ AU, rather than $r = R_{\rm A}$, since the latter quantity varies with temperature. The former quantity is approximately the value of $R_{\rm A}$ at the $T = 200$ K background temperature of our prototype simulation.

Several notable features appear in the figure. First, the time averaged spin values vary with background temperature. For the smaller enclosing sphere in particular, the highest background temperature models generate spins averaging well below zero (opposite the present day spin directions of the major planets). For the simulation with the lowest background temperature, the spin increases to an average nearly 80% that of Jupiter's present day spin normalized by mass and in the same direction. At larger radii, a similar effect occurs–the envelope spin increases, becoming much less negative as temperature decreases. The values of the spin averages fall well outside the range derived from the study of different physical models in figures 9 and 10, above, and we conclude that they signify a quantitative difference in the flow behavior in comparison to the other models in our study.

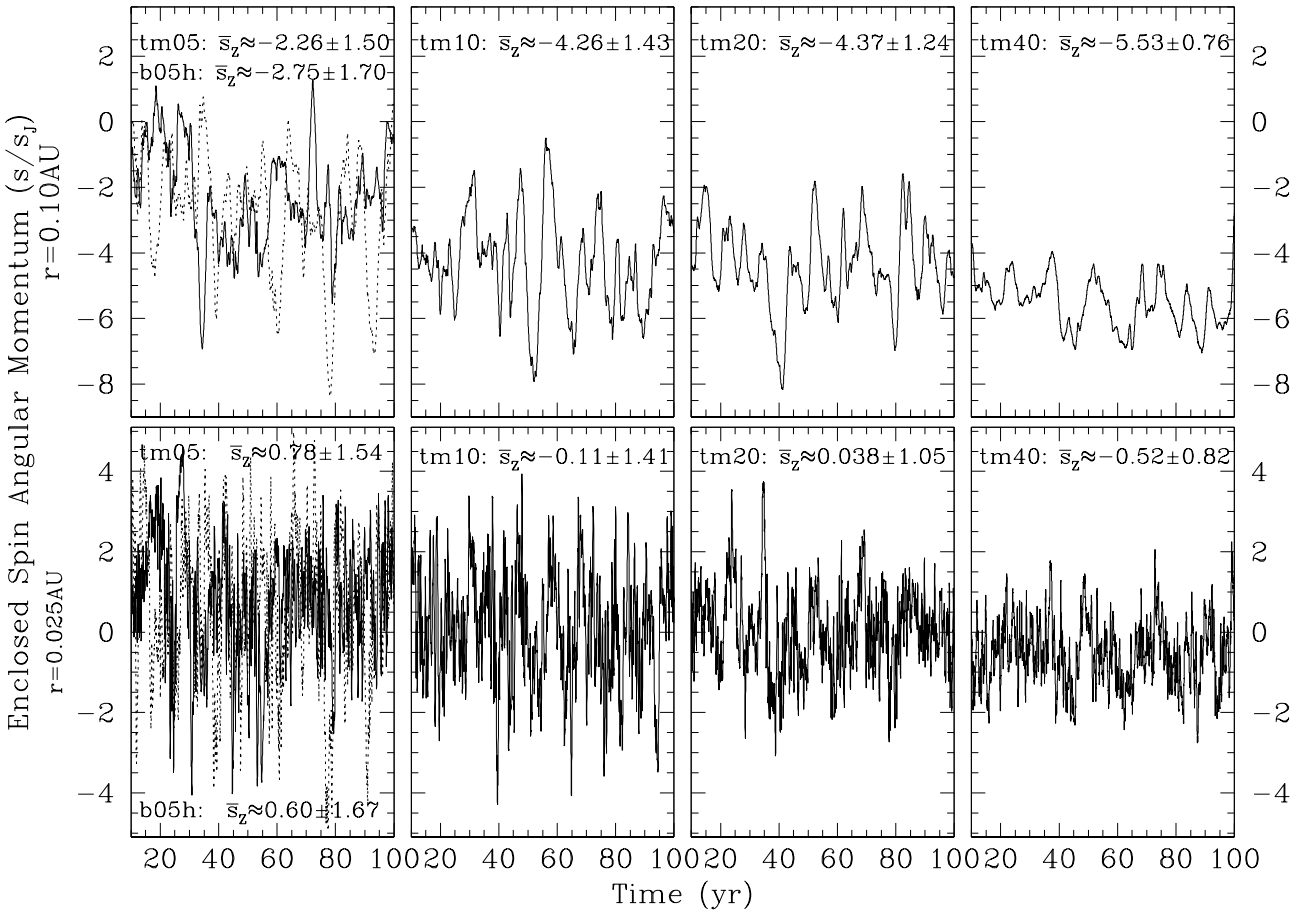

Figure 15. The z component of spin angular momentum per unit mass as a function of time, enclosed in spheres of radius $r = 0.1$ AU($\approx 0.9R_{\rm H}$) (top) and of $r = 0.025$ AU (bottom). From left to right, the panels show the simulations with background temperature $T = 50$ K, $T = 100$ K, $T = 200$ K and $T = 400$ K, respectively. In the left-most panels, simulation *tm05* is shown with solid curves, and *b05h* is shown with dotted curves.

The trend towards more negative spins at higher temperatures and more positive values at lower temperatures correlates directly with the changes in position of co-rotation relative to the core (see Table 2). For simulation *tm40*, for example, the inwards offset is largest of any in our study. By its nature, such an offset exposes the core to material with correspondingly larger relative velocities, and larger net angular momenta relative to the core. In this case, the large negative angular momentum of the material overwhelms the tendency of the system's fictitious forces to produce prograde rotation around the core, even in the regions closest to the core itself.

At the other extreme, the behavior seen in the lowest temperature simulations is consistent with the prograde rotation we would expect in the limit of a zero temperature, purely dynamical flow, expected from an ensemble of massless test particles. Even so, for the $T = 50$ K simulation, where $R_{\rm A} \sim R_{\rm H}$, the spin enclosed within the Hill volume remains negative, indicating that a significant component of material at these distances is not 'envelope' material at all, but rather merely background disk material which is passing through that volume of space. We conclude that for any temperature that we might reasonably expect to be present in the disks of forming stars, some disk material will enter the classical Hill volume and return again to the circumstellar disk.

Second, at progressively lower background temperatures, the amplitudes of the spin variations increase, particularly for the smaller enclosing sphere (bottom panels) where the variation increases by nearly a factor of two as measured by the rms deviations from the averages. The amplitude and spatial extent of density variations in the envelope shows a similar trend, as we show in figure 16. Within a distance of $\sim 1/4R_{\rm H}$from the core, amplitudes of a factor of up 2-3 in normalized "peak to peak" variation and 30-70% in variance are present in all four simulations. At larger distances, significant differences appear between the behaviors seen at different temperatures. While the variations in both amplitude and spatial extent decrease with increasing temperature in all four simulations, for the highest temperature realization they become essentially indistinguishable from the background flow within a distance of about $2R_{\rm H}$. At the other extreme, for the lowest temperature realization, variations remain significant up to $\sim 4R_{\rm H}$ from the core, and are

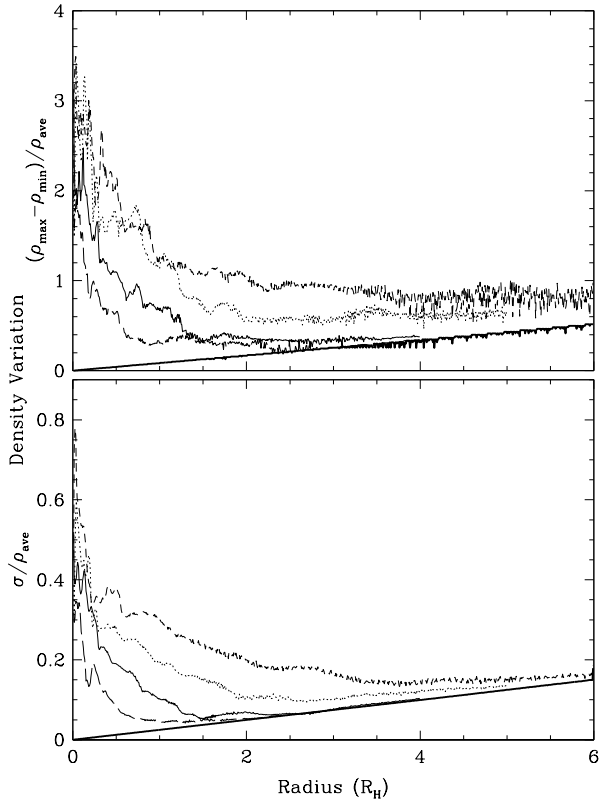

Figure 16. Variations in density as a function of distance from the core at $t \approx 74$ yr (i.e. at the same time presented in figures 2-5), for simulations with different background temperatures, using the density extrema (top) and the density variance (bottom) as metrics, both normalized to the average density at each distance. The long dashed, solid, dotted, and short dashed lines define the variations for simulations *tm40, tm20, tm10* and *tm05*, respectively. The heavy solid line defines the variations intrinsic to the background flow, which are derived from the radial gradient of density as a function of distance from the star.

non-zero all the way to the edge of the simulation volume, at $6R_{\rm H}$. The behavior of the middle temperature realizations are bracketed by those at the high and low extremes.

We attribute the increases in variability, both in spin and in density, to feedback generated by perturbed material as it returns to the envelope for one or more additional encounters. Expelled material will inevitably exhibit differences from the smooth background flow as it enters the core's environment. When temperatures are low, flow perturbations extend to larger distances and reach greater amplitudes than at higher temperatures, due to the decreased importance of pressure derived forces far from the core. These forces act to restore the flow to its background state and, when they are small, larger excursions may be sustained before the restoring forces reach magnitudes large enough to return the flow to its unperturbed state. Significantly, variability is not suppressed for any background temperature studied, and we conclude that the activity is robust.

4.4.3 Generalizing the results to other core masses

The simulations in the last section consider only $10M_{\oplus}$ cores. The results, however, can be generalized by framing them in terms of the the accretion radius, to parameterize the spatial extent of the activity, and the dimensionless ratio of the accretion radius to the Hill radius:

$$\frac{R_A}{R_H} = \frac{G(3M_*)^{1/3}}{a_{\rm pl}} \frac{M_{\rm pl}^{2/3}}{c_s^2}, \tag{23}$$

to parameterize characteristics of the flow activity. The ratio is inversely proportional to the background temperature, by way of the squared sound speed term, c_s^2, and its relationship to temperature through the equation of state. It is also directly related to the core's mass present in the definitions of both $R_{\rm A}$ and $R_{\rm H}$, resulting in the proportionality of ${M_{\rm pl}}^{2/3}$. Therefore, for a given semi-major axis, we can specify characteristics of the dynamical activity for any pair of $(T, M_{\rm pl})$ values.

We can interpret the meaning of a given ratio by recalling the physical meanings of the two quantities that define it. Specifically, the accretion radius, as noted in section 2.1.6, defines the location at which gas's thermal energy and gravitational energy of the core become comparable in magnitude. In turn, the Hill radius (or more generally, the full three dimensional Roche surface, for which the Hill radius defines the largest separation from the core) defines the locations at which the centrifugal potential energy arising from the rotating frame and the combined gravitational potential energies of the star and core become comparable. Their ratio, therefore, becomes a measure of the relative importance of the rotating frame in comparison to thermodynamic properties on the flow.

In this context, we designate the region of parameter space where the ratio $R_{\rm A}/R_{\rm H}$ is below unity, as the "thermodynamic flow regime", because the thermal energy of the background flow exceeds that of both gravitational and centrifugal potentials at the Hill radius. Therefore, the flow will be dominated by the pressure effects that define the thermodynamic state of the gas, with only small influences from the rotating frame. At smaller separations, effects of the rotating reference frame will have still smaller influence, while effects due to the gas's thermal properties increase. As gas falls deeper into the core's gravitational potential well, hydrodynamic feedback on the flow becomes important, as gravitational potential energy is converted into thermal energy. We therefore expect flow features similar to the "non-stationary" behaviors reported by, e.g., Ruffert (1997, 1999), who report flow patterns around a point mass in which the direction of rotation oscillates in time.

We designate the region of parameter space where the ratio is larger than unity, as the "celestial dynamic flow regime", because thermal energy plays a relatively smaller role at the Hill radius, so that gas flow more closely resembles that of a purely dynamical system of massless test particles. Systems in this regime will be characterized by prograde rotational flows near the core, a "horseshoe" orbit region at distances outside the separatrix defined by the Hill volume, and circulating orbits both inside and outside of the orbit position of the core. Finally, for ratios near unity, thermal energies and gravitational energies, along with the forces associated with each, are of comparable magnitudes.

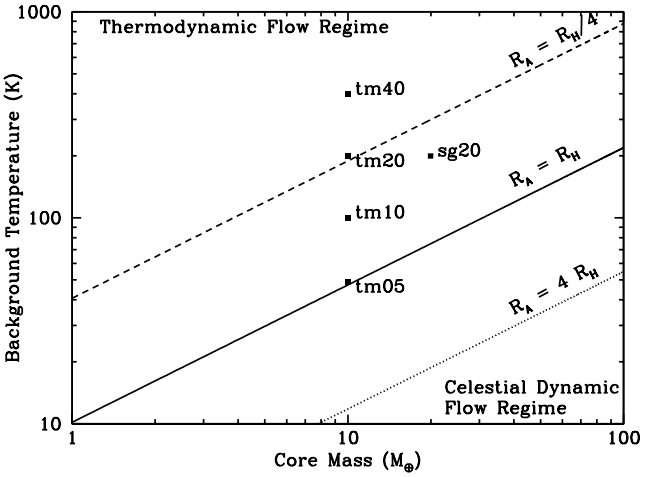

Figure 17. Lines of constant R_A/R_H, plotted in (T, M_{plan}) space, together with the loci of several of our simulations, as marked. Three lines are plotted, showing ratios of unity (solid) and ratios where R_A is four times larger (dotted) or smaller (dashed) than R_H. The regimes designated as celestial dynamic and thermodynamic flow regimes, as defined in the text, are also shown.

We therefore may expect the flow to exhibit features of both types of flow.

Figure 17 displays three lines of constant radius ratio in (T, M_{pl}) space, each assuming semi-major axis of 5.2 AU, as in our simulations. Following the discussion above, we expect flow patterns of similar character at each point along these lines, and different flow patterns as the ratio changes. Specifically, that oscillating flows are ubiquitous for all of the simulations, as expected from their placement in the thermodynamic flow regime. In addition, for lower temperatures, where the ratio lies closer to unity, the effects of the rotating frame play a larger and larger role as the time averaged spin tends toward positive, or at least less negative, values. Higher amplitude oscillations are also generated, consistent with the increased importance of the celestial dynamic effects due to the rotating frame.

Of note in the figure is that for the low core masses typical of the early stages of growth, and for temperatures of $\lesssim 150 - 200$ K, as expected in the region of core formation (i.e. the "ice line", where solid densities increase due to the formation of ices), the flow characteristics fall well within the thermodynamic flow regime. Therefore, given a background temperature near that of ice formation, we expect that a $1M_\oplus$ core will exhibit similar flow characteristics to our simulation *tm40*, with an oscillating flow pattern present in a limited volume close to the core, with low amplitude. At the same temperature, a 3-5$M_\oplus$ core would generate activity over a larger fraction of its Hill volume, with similar behavior to that of our prototype simulation *tm20*. Thermodynamic driving of the flow will become unimportant only at very high core masses or very low temperatures.

We conclude that thermodynamically active flows will be an important characteristic of core environments during their early stages of growth. The activity will only decrease in importance for objects above a few tens of earth masses in size, as values of the radius ratio increase to well above unity. Because we have not attempted simulations with such high core masses however, we cannot determine with certainty the masses for which the activity will become negligible.

5 RELEVANCE OF OUR MODELS FOR CHONDRULE FORMATION

An important implication of the temperature and density data derived from our simulations, discussed in section 3.2.1, lies well outside of the study of dynamical phenomena that may develop in the Jovian planet formation environment. Specifically, the densities, temperatures and time scales that occur in the envelope may be important for the theory of meteoritics and, more specifically, to models of chondrule formation.

Chondrules, and the meteorites that contain them, represent a large fraction of the volume of meteorites that have fallen to the earth and been studied. They are solidified, spherical melt droplets of refractory materials typically up to a few millimeters in size. Briefly summarized from Jones *et al.* (2000), we note for our purposes that chondrules underwent both a very rapid heating event to ∼2000 K, followed quickly by a rapid cooling event of magnitude 50-1000 K/hr. Among a wide variety of models purporting to produce such conditions, passage of solid material through nebular shocks is currently favored as among the most likely (see e.g. Desch & Connolly 2002). Among this model's drawbacks are, first, that shocks that have the right density, temperature and velocity characteristics are hard to form and, second, that it is difficult to arrange for these shocks to exist for a long enough time to produce enough bodies to match the current observations.

The parameter space for which chondrule production may occur in shocks is bounded by pre-shock densities within a factor of a few of 10^{-9} g cm^{-3}, temperatures near 300 K and shock speeds near 6–7 km s^{-1} (Desch & Connolly 2002, Table 5). For these conditions, the authors also note that enhancements in the particle density were important for formation models. Concurrent work of Ciesla & Hood (2002); Iida *et al.* (2001) come to similar conclusions. Figures 2 and 4 show that appropriate background conditions exist in our simulations, and we propose that dynamical activity in the Jovian envelope could provide a source for both shocks and reversible compressive heating that remedy the shortcomings noted above.

Although the basic temperature and density conditions that occur in our simulations can be seen, e.g., in figures 4 and 6, ascertaining whether short duration heating and cooling events are also present requires additional analysis. We considered and discarded the option of including test particles that could be passively advected with the local flow, because of the significant added computational and storage cost they would require. Instead, we rely on the similar–but not identical–solution of 'advecting' test particles through a fixed-time snapshot of the conditions at a specific time.

To that end, we have performed a streamline analysis of the trajectories of an ensemble of test particles injected into the simulation restart dump of our prototype model, for the same time as that shown for figures 2 and 4. Particles are placed at a set of locations at the edge of the grid and allowed to advect through the simulation volume us-

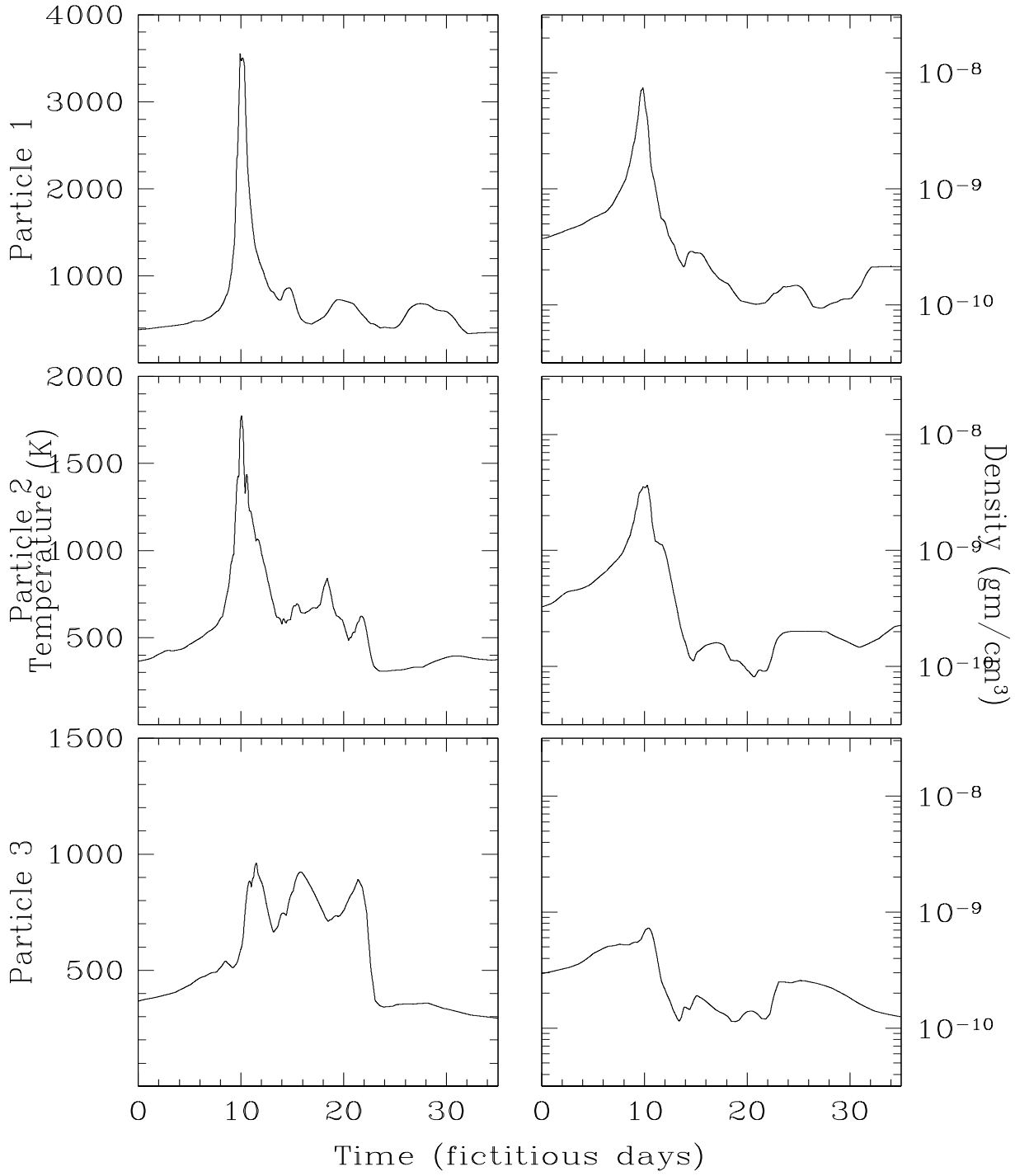

Figure 18. The temperature (left panels) and density (right panels) encountered by three test particles as they are advected through a snapshot of the simulation volume, each as functions of a fictitious time coordinate, described in the text. The zero point for time has been arbitrarily shifted in each case so that the peak temperature occurs at ~ 10 days.

ing the local fluid velocity, linearly interpolated between the grid zones adjacent to the particle at each time. Each particle is given a time step based on that used to advance the gas at that location, so that it advances forwards through a fictitious time coordinate, passing through the volume at the rate of matter in the local flow. Similar linear interpolations of density and internal energy are used to derive the temperature from the equation of state.

In Figure 18, we show temperatures and densities for three test particles for which a passage through the environment of the core has occurred. The particles shown were chosen to illustrate the range of peak temperatures and den-

sities that may be encountered by slightly different trajectories through the envelope. Each encountered a short duration heating and cooling event as they passed through the dynamically active region close to the core, but the magnitudes and duration varied in each case. In the top example (test particle 1), the peak temperature rose to well over 3000 K and the density to nearly 10^{-8} g cm^{-3} as the particle's trajectory passed through the innermost regions of the envelope. The conditions encountered by the particle 2 were much more moderate, with peak temperature and density values of $\sim$ 1800 K and 4×10^{-9} g cm^{-3} respectively. Particle 3's trajectory took it only through the outer portion of the envelope, so that it encountered only much lower temperatures and densities, although in this case for a much longer period of time than either of the other two cases shown. All three particles encountered several days of cooler processing near 500-800 K, and a visual scan of many other similar events shows that such additional annealing is common.

The temperature peaks for test particles 1 and 2 offer widths of $\lesssim 1$ day, with both a very rapid rise and fall. Close examination of their trajectories reveal that the widths reflect essentially the crossing time for a single grid zone in the simulation. Therefore, although already quite narrow, they are actually likely to be overestimates of the true widths that would be obtained from the same models realized at still higher resolution. The dynamical activity in the envelope, coupled with the temporally very narrow temperature/density peaks, especially in cases similar to that of particle 2, offer evidence that chondrule production could occur in the environment of Jovian planet formation.

6 DISCUSSION

6.1 Summary of our main results

We have performed a suite of 3D numerical simulations of a cubic 'cutout' region around a $10M_\oplus$ point mass embedded in a circumstellar disk, in a modified shearing box framework. We find that the flow is not characterized by a simple one dimensional circumplanetary envelope embedded in a near static background flow. Instead it is highly dynamic, varying on time scales ranging from months to years far from the core, down to hours or days, very close to it.

We used the RMS amplitude of time variations observed in components of specific angular momentum of material flowing around the core as a quantitative proxy for this activity and studied its sensitivity to changes in physical and numerical parameters used to model the evolution. Specifically, we varied the character of the core, via its mass and gravitational softening coefficient, and we studied the sensitivity of the activity to artificial changes in the background flow, imposed by changes in the overall temperature or density gradients in the disk, imposed by changes in the background temperature of the disk, or imposed by changes in the assumed equation of state. We found that the amplitude is sensitive to the character of the core, increasing with core mass and decreasing with larger gravitational softening. Increases in the background temperature of the disk cause decreases in both the amplitude and spatial extent of the activity. Activity can also nearly be suppressed when we assume a fixed equation of state–either isothermal or isentropic–which in turn serves as a proxy for more complex heating and cooling processes neglected in our current work. Each of these factors contribute to the efficiency and character of hydrodynamic feedback on the large scale flow by the material returning to the background after encountering the core and we conclude that the origin of the activity is closely linked to such feedback.

Finally, we demonstrate that an important consequence of the dynamical activity is to generate very short duration heating and cooling events in material that travels through the envelope. We compare conditions in these events to those expected to be required to form chondrules, and show that the ranges of temperatures and densities reached span those for which chondrule formation is expected. They also extend to longer duration and lower temperature events for which significant annealing may occur, and we propose that the origin Jovian planets and the origin of of chondrules and other annealed solids in the solar nebula are linked, through the dynamical activity in the envelope. If such a link can be established, then chondrules and annealed solids represent a physically examinable record of the processes present during the formation of Jovian planets.

6.2 Potential implications of our results

Our models represent a significant step towards a complete picture of the formation of Jovian planets in the context of the core accretion model. All of our simulations generate some dynamical activity and only simulations evolved using fixed EOS evolution or large gravitational softening produce activity of significantly lower magnitude than in our prototype simulation and its many variations. Given the severe and unphysical restrictions on the thermodynamics imposed by fixed EOS evolution, we do not believe that the results of those simulations closely resemble the actual evolution of any real system. A large gravitational softening parameter is similarly restrictive, because it implies a spatially extended and relatively massive envelope, at very early phases of the core's growth. We therefore believe that more sophisticated models will show that dynamical activity will be present at levels important enough to play a role in overall formation process of Jovian planets. If so, our results mean that the standard core accretion model for Jovian planet formation will require revisions, to include the effects of such dynamical activity.

Given this statement, we now speculate on what those effects may be, and their contribution to the planet formation process. Most importantly, we expect the mass accretion rate to differ from that derived in the context of the standard core accretion model, because in that model the accretion is throttled by the rate of energy loss from the outer surface of the envelope. When the rate is low, pressure forces build up and choke off further accretion, when it is high, accretion proceeds more quickly. However, if the envelope has no stable outer surface, high pressures at any point on the 'surface' (such that one can be defined at all) will not hinder material flow through an adjacent region where they are low. Indeed, such high and low pressure regions may simply be consequences of material flowing into or out of the core's environment. They may also be consequences of thermal energy generation from shocks created by interacting

material flows. In this case, an accurate model of the evolution will require an accurate accounting of the contributions from such energy generation and advective terms, to both the mass accretion and energy loss rates of the material in the core's environment.

Depending on its strength, dynamical activity may either delay accretion, by repeatedly disrupting the formation of the envelope, or enhance it, by driving instabilities in the flow. In the context of our current models, we cannot determine which outcome is more likely, or if both occur at different times. If the envelope is disrupted on timescales short compared to its cooling timescale, then our present models, which neglect cooling entirely, will provide an accurate picture of the long term flow pattern. Any material which does cool will be swept away, rather than becoming a permanent part of the core's envelope. If instead instabilities occur which do *not* entirely disrupt the envelope, a likely consequence will be rapid mass and angular momentum transport through the envelope onto the core. Instabilities are known to develop in rotating polytropes (Pickett *et al.* 1996; Toman *et al.* 1998), morphologically similar to the planet formation environments discussed here, but whether those or other, similar instabilities can be triggered in the present context awaits further study. Also, the consequences of such rapid accretion are unclear. How quickly would a massive envelope develop in which further activity did not play a large role?

The scenario we present offers a number of attractive advantages over other models of Jovian planet formation. Unlike both the class of formation models using global gravitational instabilities in the circumstellar disk and of many previous models of core accretion, a massive disk is not required at any time during the evolution. In particular, no massive disk is required to exist for the long period of time required for the classic picture of core accretion, for which most gas accretion occurs only at the conclusion of a long hydrostatic growth period. Assuming that the activity results in enhanced mass accretion rates, it also provides a formation mechanism which avoids one of the most critical unsolved issues in standard models of core accretion, that the core does not grow quickly enough to avoid migrating through the disk and onto the star. Finally, our scenario naturally provides a mechanism for producing very short duration heating and cooling events with thermodynamic characteristics similar to those expected to produce chondrules and annealed solids. Production in this scenario will endure for a significant fraction of the formation time scale of Jovian planets (itself a significant fraction of the disk lifetime), resulting both in a large yield of objects and allowing both processing and reprocessing events to occur, both factors consistent with the meteorite record.

6.3 Comparisons to other work

The work described in this paper can be profitably compared to three main categories of research on Jovian planets. Together they make up a spectrum of models ranging on one extreme, to multidimensional models which explore the interaction of a circumstellar disk with a massive object embedded within it, using relatively simple physical models (Lubow *et al.* 1999; D'Angelo *et al.* 2002, 2003b,a; Bate *et al.* 2003), and on the other extreme, to one dimensional models which explore the core accretion paradigm using highly detailed physical models (Pollack *et al.* 1996; Alibert *et al.* 2004; Hubickyj *et al.* 2005; Helled, Podolak & Kovetz 2008; Terquem & Heinemann 2011; Lissauer *et al.* 2009). In the middle lies a class of work most similar to ours Ayliffe & Bate (2009); Rafikov (2006); Papaloizou & Nelson (2005); Machida *et al.* (2008); Tanigawa, Ohtsuki & Machida (2012), in which special attention is paid to the interactions between the envelope and the surrounding disk.

The main focus of most previous multi-dimensional work has been on large scale interactions between the core and the disk as a whole, in order to study the migration of the core through the disk and determine parameters related to its survival. In this context, many details of the structure of the envelope become less important, and approximations are made to sidestep the more difficult numerical and physical issues. In comparison, our focus has been primarily on the interaction of the envelope with the core and the immediately surrounding disk material. Accordingly, we provide only a rudimentary description of the background disk, through a boundary condition and through its gravitational effect on the material inside our simulation volume. We concentrate our spatial resolution on the envelope region only, thereby permitting much finer resolution of the flow features. The work presented here represents the highest resolution simulations studying the formation of Jovian planets so far published. Our work also includes a physical model which, while necessarily more simple than required for a complete picture of the evolution, at least avoids some of the most restrictive assumptions of previous models.

As noted in section 3.1, the morphologies found in our work differ from those of the previous studies, exhibiting both more dynamical activity and less disk-like or spiral structures in the circum-core environment. The reasons for the differences between the morphology most likely lie in differences in the physical assumptions made in each. Specifically, the most important assumptions include those regarding the thermodynamic treatment for the gas, those regarding its distribution around the core and those regarding the continued mass accretion onto the core itself. We now discuss the physical implications of each of these assumptions.

We employ an ideal gas equation of state to close the system of hydrodynamic equations. Additionally, no sources of heating or cooling are included apart from shock heating generated by the dynamical interactions of the flow on itself. In contrast, many previous workers have chosen an isothermal equation of state, which artificially (and very efficiently) removes thermal energy generated by those same interactions. High temperatures and pressures are therefore suppressed, and the feedback loop that would otherwise exist as the hot gas perturbs incoming material cannot form. As we showed in section 4.4.1, our simulations do not exhibit dynamical activity when an isothermal equation of state is used, consistent with the lack of such activity in other work. A complete model will of course include some cooling effects due to radiation, which will undoubtedly act to suppress the activity we see, however the magnitude of this effect is difficult to estimate from the currently available literature.

Although some calculations have been performed (AB09) which include radiative cooling, they do not super-

sede our results due to limitations implied by the resolution afforded by the simulations themselves. Their spatial resolution, although high in relative terms, is still much lower than is required resolve the flow sufficiently at small distances from the core to capture the extremely small scale features that characterize the shocks and dynamical activity close to the core. For example, tests of the shock capturing characteristics of the PPM algorithm in use in our simulatons, show that shocks can be resolved with a maximum of 2-3 grid zones, corresponding to distances of $\lesssim 2R_J$ at the grid zoning used in our simulations. In contrast, the SPH ('Smoothed Particle Hydrodynamics') method used by AB09 requires at least 5-10 particle smoothing lengths to resolve a shock (see, e.g., section 6 of Price 2012). While AB09 quote a minimum smoothing length over their simulations comparable to our zone size, their overall particle count is quite low, implying that very few particles have such small sizes, while most are much larger. Coupled with the comparatively large artificial viscosity required by the method, we believe that the features we observe in our simulations would not have been observable in theirs, independent of any considerations regarding cooling.

Our work assumes that no gas has accumulated around the core. This assumption manifests explicitly in our initial conditions, for which we define only a 'bare' core embedded in an unperturbed background flow, and implicitly through our specification of the gravitational softening of the core. In addition to its normal purpose as an aid to sidestep various numerical issues in finitely resolved simulations, using non-zero gravitational softening is equivalent to the assumption that the core's mass is distributed over a finite spatial volume, corresponding to the spatial scale of the softening (see, e.g., D'Angelo *et al.* (2003a) for a particularly detailed discussion of such softened potentials). The gravitational softening used our simulations is smaller than employed in many other works, where simulations with values of $\sim R_{\rm H}/10$–$R_{\rm H}/5$ are typical (e.g. D'Angelo *et al.* 2003a). In contrast, the largest softening we use in any simulation is $\sim R_{\rm H}/8$ (for simulation *so10*), while in all others at the same resolution it is a factor 16 smaller. Given the results of section 4.2, where we showed that softening values this large are sufficient to suppress dynamical activity, we conclude that other published work would not have seen such activity, due to the differences between their assumptions and ours.

Further, the effect of permitting the core to accrete essentially all material moving into a small volume around it is to suppress any buildup of gas in the envelope. Such buildup would otherwise provide a back pressure and either stall further accretion or, as happens here, provides a supply of material with which additional infalling material can interact. For simulations of cores with sufficient mass, well above that expected to cause the onset of 'core instability' (Wuchterl *et al.* 2000), unimpeded accretion may be a physically relevant and important process to consider. In the present case however, where we study the evolution around only $10M_\oplus$ cores with very low mass envelopes, such an assumption is not valid. Unimpeded accretion is also physically inconsistent with the existence of the massive envelope implied by the large gravitational softening parameters, since any such envelope would quickly be accreted into the core itself.

Our spatial resolution is nearly fine enough to resolve the core (see section 2.1.5). In this context, implementing a 'black hole' accretion model, in which all material moving into a predefined volume around the core is accreted, would be inconsistent with the known character of the core (i.e. that it is solid). Such material becomes unavailable to interact with other material falling onto the core at later times. Therefore, models in which accretion is permitted may unintentially suppress the feedback loop that generates the vigorous dynamical activity we observe in our simulations.

Previous 1D work focuses primarily on the secular growth of the envelope and core over its long term (10^5-10^6 year) evolution. It therefore includes detailed treatments of physical processes relevant over long time scales, while assuming that short term dynamical fluctuations average out over time. In comparison, our models include a simpler physical model but fully 3D spatial resolution. Due to the computational cost of 3D models however, our simulations extend over an very short period of the total evolutionary history of the planet's growth.

Each of these 1D models still requires that a boundary condition be applied at the outer edge of the envelope. To the meager extent that defining an envelope can be meaningful in the simulations we present, our dynamical results are broadly consistent with the condition assumed in the Lissauer *et al.* (2009) simulations, in which the boundary was defined at a radius of $\sim R_{\rm H}/4$ from the core. The Lissauer *et al.* (2009) assumption is based on the result of dynamical calculations somewhat similar to our own (D'Angelo *et al.* 2003a), in which only tracer particles closer than $R_{\rm H}/4$ from the core remained near it. Our simulations do not form any envelope structure, and material in the volume that they define as most strongly bound to the core is most dynamically active in our simulations. We do however, concur with the result that material at larger separations (still within the Hill volume) is largely composed of background disk material whose trajectory has merely caused it to pass near the core, rather than become bound to it. This same result is inconsistent with that of Terquem & Heinemann (2011), who find that the volume of gas that is bound to the core will grow to fill its entire Roche lobe even if it initially fills only some fraction of it.

An important concern regarding all 1D models is the issue of whether or not the assumption that hydrodynamic properties of the system actually do average out over time, so that a hydrostatic evolutionary model is accurate. Do hydrodynamic effects force the evolution to proceed in a direction that it otherwise would not have taken, considering only the hydrostatic properties of the system? Our 3D models illustrate that the formation environment for Jovian planets cannot be adequately described by any hydrostatic treatment. Such a treatment would imply that material and energy transfer between the envelope and disk occurs through a stable boundary, with material far from that boundary being only indirectly affected. On the other hand, our simulations show that the interactions between disk and envelope frequently disrupt the envelope entirely, so that its growth must begin again from scratch. Also, with such vigorous activity, cooling by any process becomes far less relevant, since the cooled material does not remain near the core for long enough to affect the long term evolution of the envelope. Since our simulations extend over only a tiny fraction

of the total formation history of Jovian planets and also do not incorporate a sufficiently complete physical model of the evolution, we cannot yet speculate as to the fraction of a planet's formation history such a statement will be true. In the following two sections, we discuss the implications of such activity on current core accretion models, and the components of physical models that we believe will be required to make such conclusions.

7 UNANSWERED QUESTIONS

The physical model included in our work is a necessarily simplistic view of the actual environment of forming Jovian planets and, because of that, our work generates more questions than it answers about the growth of Jovian planets and solar system formation. In this section, we point out a number of such simplifications in our models, discuss what we believe is the relative importance of each in the context of Jovian planet formation, and pose a number of questions that can be addressed as they are removed.

7.1 Simplifications that affect the thermodynamic state of the envelope

We made two simplifications in this work which appear to be critical to making definitive connections between our results and the physical systems they are intended to model. Each of these factors contribute directly to models of the internal structure of a hydrostatic (or nearly so) envelope, determining its energy balance and its density and temperature structure as a function of radius. They are critical components of both hydrodynamic and hydrostatic models in this context. Before any detailed analysis of the conditions will be of lasting value for theories of planet formation, each must be accurately accounted for, particularly in the deeper regions of the envelope where dynamical activity is most vigorous.

First, no account has been taken of the radiative cooling and heating processes that undoubtedly occur in the envelope, beyond our models employing fixed equations of state. As discussed in the context of the possibilities for gravitational instabilities to form planets (Durisen *et al.* 2007), use of fixed equations of state as proxies for cooling models greatly restricts the behavior of the energy balance in the gas. Whether or not these restrictions correctly represent the actual heating and cooling behavior of the Jovian envelope and its environment, or instead artificially suppress the activity which should actually be present, must be addressed in follow-up work.

In our simulations, the envelope volume is characterized both by high temperatures and densities and by rapid changes and large gradients of the same quantities. It seems likely that including the effects of radiative transfer will tend to smooth out temperature gradients throughout the system. How much so, and to what extent are the temperatures and densities artificially altered from their actual values by our physical model? To what extent will the dynamical properties of the system will change when they are included? Will the dynamical activity continue? Will shocks still develop in the flow? Preliminary indications with the comparatively extreme restrictions of locally isothermal and locally isentropic equations of state suggest that at least some activity remains, so we remain hopeful that our current treatment is approximately correct.

Unfortunately, the material opacities needed to model radiative transport accurately are poorly constrained, since they arise largely from the properties of ice and dust, both in terms of grain sizes distribution and in terms of their composition. In many regions throughout the envelope, solids may be vaporized either temporarily or permanently, causing opacities to change by orders of magnitude over small spatial and temporal scales. When solids are removed as opacity sources, the envelope may become optically thin so that radiative cooling becomes more efficient, particularly closer to the core where temperatures are highest. Will radiative cooling in these regions redistribute or remove enough energy from the gas to change the activity that occurs when radiative processes are neglected? Moreover, when they reform, grains with similar chemical compositions may have quite different opacities than originally. Radiative transfer models which incorporate this grain history will likely require the advection of tracers in the simulations, which model different chemical compositions of different solid species. This is challenging, both in the context of developing a physical model and numerically. To what extent will such models affect the dynamics?

Second, no account has been taken of the temperature and density dependence of the equation of state. Including a complete equation of state will also cause important changes to the flow because, at various temperatures, the adiabatic exponent, γ, of the gas will differ from the constant value of $\gamma = 1.42$ that we have assumed. While this value will be approximately correct for temperatures relevant for the background circumstellar disk material (i.e. $T \sim 100 - 1000$ K), where at various temperatures rotational and vibrational modes of hydrogen molecules play a greater or lesser role, it becomes much less so for higher temperatures and densities characteristic of the gas deep in the envelope near the core. Above $T \sim 1500 - 2000$ K, dissociation and ionization become increasingly important, and the effective adiabatic exponent falls to values as low as $\gamma \sim 1.1$, before increasing again to $\gamma = 5/3$ when the gas becomes fully dissociated. As shown in figure 4, the envelope temperatures span this range. For a given compression, a lower adiabatic exponent means that pressure increases by a smaller amount. Therefore, our fixed exponent treatment may artificially increase pressure gradients beyond the physically relevant levels they should reach, thereby artificially stimulating dynamical activity to a greater than realistic extent. On the other hand, lower exponents mean that a given compression event can increase the mass density to a higher values, perhaps to levels at which self gravitating instabilities can develop. Which overall effect will dominate?

Once these thermodynamic effects are included, it will be of interest to run simulations for far longer in time, in order to explore questions relating to whether activity continues indefinitely or instead decays with time. Our current models simulate only a 100 yr segment of the Jovian planet formation history, during a time when the envelope did not contain much mass. Because there were no energy loss mechanisms in our current models, no mass accretion into the envelope could be expected. Will dynamical activity continue

to overwhelm net mass accretion onto the core, will activity continue while superposed upon an overall net accretion rate (and at what rate?), or will the activity simply decay over time to levels unimportant for the evolution?

Over such long timescales, A third simplification of some significance to the thermodynamics will also play a role. Namely, the effect of heating due to planetesimals infalling into the envelope. Over the short periods simulated in our models, such heating is not likely to play a large role in the dynamical state, because only a few events occur during such a short time and because the energy input from any single event is not a large fraction of the internal energy of the envelope. Such conditions will not be true over longer periods, during which many more events occur. How will dynamical activity change when this additional heating source is accounted for? In our current simulations, disk material enters the envelope then leaves it again, carrying with it thermal energy generated in shocks or other interactions with material near the core. Will a similar outcome hold for the heating generated by an infalling planetesimal, or will the additional thermal energy be trapped in the envelope, escaping only slowly to the background disk?

Longer simulations will permit studies not only of the accretion rate, but also of the envelope's behavior as it becomes more massive. Does activity depend on having only a low mass envelope? Does activity enhance the net accretion rate or reduce it? An answer to this question is important in the context of the overall survival of a proto-planet because the observed lifetimes of the circumstellar disks out of which planet form may only be 2–4 million years (Haisch *et al.* 2001), while core accretion models (Pollack *et al.* 1996) require as many as ∼6 million years even in a relatively massive massive disks (2–3 times the minimum solar nebula).

7.2 Simplifications in the initial conditions and the physical realization of the disk and core

In addition to the simplifications in the thermodynamic treatment, our models also study only a limited range of the parameter space of interest in terms of the initial conditions explored. They employ simplified treatments of several physically relevant components of the overall system, such as the treatment of the core itself, and the vertical structure of the disk.

In this work, we have studied the flow around only $10M_\oplus$ cores, but such objects must first, of course, grow from smaller masses. Will dynamical activity occur in the flow around lower mass cores? The discussion in section 4.4.3, would suggests that activity will occur, but would be less vigorous for the smallest cores for conditions typical in the parts of the disk where cores are expected to form. Is there a lower limit below which activity does not play an important role in the evolution? If the character of mass accretion also changes markedly with the strength of the dynamical activity, then an important observable consequence of such a limit would be the present day masses of the Jovian planets in our solar system. Can such a correlation be made?

Due largely to limits imposed by computational cost, we have approximated the core as a softened point mass with no actual size or surface. With only a factor of ~ 2 increase in spatial resolution from the highest employed here, simulations would begin to resolve the core and some, more physical, accounting must then be made of its structure. We forsee that a simple solid surface realized by a reflecting boundary condition will be the next step, and will provide a physical picture adequate to model the influence of the core's spatial extent on the flow. Of interest will be the question of whether or not interactions with the surface enhance dynamical activity, perhaps by being reflected off of it to interact with other infalling material. Also, the gravitational potential well reaches its maximum depth at the core's surface. Resolving the flow there means that the temperatures and densities seen close to the core will represent the most extreme of those expected in any dynamical flow. Will some fraction of such material also be ejected into the background disk flow? Will it carry signatures of its passage through the core environment?

A still more complex treatment of the surface would require models of the interaction between the material in the core and the flow. To what extent does mass exchange between the core and envelope occur? Does high-Z core material mix into the envelope, (and perhaps also back out into the disk itself?), thereby enriching it, or does it remain largely unaffected by the envelope activity? Does such mixing change with envelope mass?

Indirectly, the accretion rate will also influence the migration rate of the core through the disk. As its mass increases, the mutual gravitational torques between the core and disk will increase in turn and the core interacts more strongly. Whether the stronger interaction leads to increased migration will depend on details of the mass distribution around the core. Accounting only for torques from Lindblad resonances (see e.g., Ward 1997a), migration will accelerate. Accounting for corotation torques as well, migration may decelerate or even reverse direction (Peplinski, Artymowicz & Mellema 2008a,b).

While omitting gravitational forces in the z coordinate precludes a description of the disk's vertical structure, we expect that the influence of that structure on the envelope activity will not be large. Here again, the activity is limited only to the immediate environment of the core, a factor of several in spatial extent smaller than the disk's scale height. A possibly more important consequence of such a treatment will be the possibility of mass being ejected entirely out of the disk, to fall later on some region distant to the core. In this case, the question of how large the accretor must be before it first begins to deplete mass from an entire vertical column of the disk. For an accretor of that size, accretion may be reduced due to the loss of material accreting onto the poles of the proto-planet and a gap may form due to the accretion of most of the material near the planet, also slowing additional migration through the disk.

Of somewhat lesser importance for the near term are the geometric approximations imposed by our choice of coordinate system and our omission of background gravitational forces in the z (vertical) coordinate of our disks. Mitigating the importance of both cases, is the fact that activity is limited to a comparatively small volume close to the core. Therefore, the coordinate system itself plays only a small role.

7.3 Is there a connection between models of Jovian planet formation models and models of chondrule formation?

As noted above, a consequence of dynamical activity in the envelope is that material is not irrevocably bound to the core after first entering the envelope environment. Instead, some fraction of the material returns to the circumstellar disk from which it originated. Will this material retain a signature of its passage through the hot, circumplanetary region? The possibility is intriguing because if so, some such material could still exist today, potentially providing a record of the conditions present during the formation of Jovian planets that could be directly observed. In fact, a common class of meteorites–chondrites–exist (see e.g. Palme & Boynton 1993) and are found throughout the solar system, which exhibit signatures of high temperature processing on time scales of only a few hours or days. Can the formation of Jupiter actually be linked to the formation of chondrules observed in the meteorite record though a model such as ours? Can it be linked to the formation of other materials, such as the annealed silicates found in comets (Harker & Desch 2002), for which the required temperatures and densities are lower?

Although the results from our initial streamline analysis are promising, they are no substitute for an investigation of the trajectories of specific packets of material through the system. In order to establish any real connection, we must perform a much more detailed analysis of the conditions encountered by such packets. Is a particle's thermodynamic trajectory the same when it is advected through an actual time dependent flow, as opposed to the fictitious advection through a fixed flow that we have performed? Will more detailed analysis show that the shocks that are generated fit into the required density/temperature/velocity parameter space? One concern already apparent is that the flow velocities of material flowing through the shocks (1-2 km s^{-1}, as estimated from the directly available fluid flow velocities themselves) are uncomfortably low compared to those quoted by Desch & Connolly (2002) and Iida *et al.* (2001). It seems unlikely that the velocities will be increased as dramatically as that by any of the improvements to the models we might make. Finally, what fraction of material encounters conditions appropriate for chondrule formation during its passage, in comparison to material that instead encounters regions that are inappropriate? And what fraction of the total budget of solid material in the solar nebula undergoes such processing? Equivalently, do conditions appropriate for chondrule formation exist for a large or small fraction of the disk lifetime, so that a larger or smaller fraction of solids encounter those conditions during their evolution? Finally, how do processed materials get from where they form (near 5 AU) to their final locations, in meteorites throughout the inner solar system?

7.4 Future Directions

We believe the most profitable course following this work will be to investigate the character of activity that is generated for cores of different masses, in order to confirm directly the scaling relationship discussed in section 4.4.3. In parallel with this effort, models employing an accurate equation of state for the circumstellar material will be of great interest. Such an equation of state must include the various molecular and atomic states of hydrogen, which will likely cause changes to the strength of the hydrodynamic feedback through the changes they imply for the ratio of specific heats, γ. Ultimately however, we expect that models including radiative transfer will be required to accurately model the full process of mass flow and accretion in the neighborhood of forming planetary cores. In future work, we hope to explore all of these questions.

APPENDIX A: DIFFERENCES FROM THE STANDARD SHEARING SHEET FORMALISM

The differences between the standard shearing sheet model and our modifications to it are to be found in the equations of motion in the x and y directions, equations 3 and 4, corresponding to an underlying radial and azimuth coordinate frame that is rotating with the angular speed of the core. Additional differences are found in the specification of the boundary treatments, as discussed in section 2.3 above. To illustrate the differences in mathematical formalisms we show here the approximations underlying both our formalism and the shearing sheet and their differences, starting from the equations of motion in a non-rotating cylindrical coordinate frame.

In an inertial, cylindrical coordinate frame, the equation of motion in the radial and azimuthal directions are

$$\frac{\partial(\rho V_r)}{\partial t} + \frac{\partial(\rho V_r V_r)}{\partial r} + \frac{\partial(\rho V_r V_\phi)}{r\partial\phi} + \frac{\partial(\rho V_r V_z)}{\partial z} - \frac{\rho V_\phi^2}{r} = -\frac{\partial p}{\partial r} - \rho\frac{\partial \Phi}{\partial r}, \quad \text{(A1)}$$

and

$$\frac{\partial(\rho V_\phi)}{\partial t} + \frac{\partial(\rho V_\phi V_r)}{\partial r} + \frac{\partial(\rho V_\phi V_\phi)}{r\partial\phi} + \frac{\partial(\rho V_\phi V_z)}{\partial z} + \frac{\rho V_r V_\phi}{r} = -\frac{\partial p}{r\partial\phi} - \rho\frac{\partial \Phi}{r\partial\phi}, \quad \text{(A2)}$$

where the capital letters on the velocities are used to denote the inertial frame velocities. In equation A1, the $\rho V_\phi^2/r$ term defines an analogue of the centrifugal force which, mathematically, comes from the fact that the full time derivative of the momentum includes components that account for the fact that direction vectors $\hat{r}$ and $\hat{\phi}$ are dependent on position and through them, also time. In equation A2, the $\rho V_r V_\phi/r$ term plays a similar role, as a near analogue of the Coriolis force.

When translating to a frame rotating at angular velocity $\Omega_{\rm fr}$, we must include centrifugal and Coriolis terms of the form $\mathbf{\Omega}_{\rm fr} \times (\mathbf{\Omega}_{\rm fr} \times \mathbf{r}) - 2\mathbf{\Omega}_{\rm fr} \times \mathbf{v}$. Additionally, the meanings of each of the variables as defined above changes, to reflect the moving coordinate system. For purposes of clarity, we note the identifications ($V_r \rightarrow v_r, V_\phi \rightarrow r\Omega_{\rm fr} + v_\phi, V_z \rightarrow v_z$) for each of the coordinate direction. In other words, lower case variable names denote quantities in the moving frame. Then, the form of equations A1 and A2 change to include the additional terms as follows:

$$\frac{\partial(\rho v_r)}{\partial t} + \frac{\partial(\rho v_r v_r)}{\partial r} + \frac{\partial(\rho v_r v_\phi)}{r\partial\phi} + \frac{\partial(\rho v_r v_z)}{\partial z} - \frac{\rho v_\phi^2}{r}$$

$$-2\rho v_\phi \Omega_{\rm fr} - \rho r \Omega_{\rm fr}^2 = -\frac{\partial p}{\partial r} - \rho \frac{\partial \Phi}{\partial r}, \qquad \text{(A3)}$$

and

$$\frac{\partial(\rho v_\phi)}{\partial t} + \frac{\partial(\rho v_\phi v_r)}{\partial r} + \frac{\partial(\rho v_\phi v_\phi)}{r\partial \phi} + \frac{\partial(\rho v_\phi v_z)}{\partial z} + \frac{\rho v_r v_\phi}{r} + 2\rho v_r \Omega_{\rm fr} = -\frac{\partial p}{r\partial \phi} - \rho \frac{\partial \Phi}{r \partial \phi}. \qquad \text{(A4)}$$

The cross term in equation A3 arises from the Coriolis term, $2\mathbf{\Omega}_{fr} \times \mathbf{v}$, while the first and third terms come from the centrifugal forces due to the curvi-linear coordinate system and the rotating frame, respectively. Together, the three terms in eqution A3 form a perfect square identical to the corresponding single term in equation A1. We complete the specification of the equations of motion defined in equations 3 and 4, by replacing the cylindrical coordinate variables $(r, r\phi)$ with (x, y).

In both the treatment above and the shearing sheet, the identification of the coordinates pairs (x, r) and $(y, r\phi)$ is made in each of the hydrodynamic equations. The shearing sheet approximation goes further than this by omitting the Coriolis-like term due to the curvature of the coordinate system (i.e. the term $\rho v_r v_\phi / r$, above) and expands the sum of the centrifugal force and the gravitational force of the central star in a Taylor series, for which the zeroth order term is assumed to be zero, and only the linear term is retained. Hawley, Gammie & Balbus (1995) state the form of the equations to be solved in the shearing sheet approximation, cast as partial derivatives of velocities. For comparison to the form used here, we recast these equations in momentum form, omitting all terms relating to magnetic fields, which we neglect entirely:

$$\frac{\partial(\rho v_x)}{\partial t} + \frac{\partial(\rho v_x v_x)}{\partial x} + \frac{\partial(\rho v_x v_y)}{\partial y} + \frac{\partial(\rho v_x v_z)}{\partial z} - 2\rho v_y \Omega_{\rm fr} = -\frac{\partial p}{\partial x} + 2\rho q \Omega^2 x \qquad \text{(A5)}$$

$$\frac{\partial(\rho v_y)}{\partial t} + \frac{\partial(\rho v_y v_x)}{\partial x} + \frac{\partial(\rho v_y v_y)}{\partial y} + \frac{\partial(\rho v_y v_z)}{\partial z} + 2\rho v_x \Omega_{\rm fr} = -\frac{\partial p}{\partial y} \qquad \text{(A6)}$$

where $q = -\partial \ln \Omega_{\rm fr} / \partial \ln r \approx 3/2$, for a nearly Keplerian disk. The last term on the right hand side of equation A5 defines the first order approximation to the effective potential in which the gas flows noted above. Rather than use this Taylor expansion approach, we retain the full form of the background potential of the star and disk, assuming only that it is constant in time. This permits a direct specification of the gravitational potential to be made, rather than an analytic approximation. It also permits transient velocity fluctuations that temporarily upset the assumption that centrifugal and gravitational forces are in equilibrium to be accounted for more fully.

APPENDIX B: NUMERICAL ISSUES REGARDING TREATMENT OF THE BOUNDARIES

The simplest method of producing a flow-out boundary in either the inner or outer x ('radial') direction would be to reproduce the flow variables of the last interior grid zone in the boundary cells adjacent to that zone and just outside the grid. We have found this method unsatisfactory for our simulations because the background state is effectively a dynamical equilibrium condition rather than a static equilibrium condition. Implementing the simplest flow-out boundary changes the gradients there (e.g. the pressure gradient partially responsible for the underlying rotation curve), and is equivalent to violating the dynamical equilibrium condition. The effect of an initially small outflow at the negative x boundary, corresponding to the inner radial boundary of the underlying disk, is to flatten the gradient and further strengthen the outflow. At the positive x boundary a flattened gradient has the opposite effect: the effect of an initially small outflow is to temporarily create a very strong, local *inflow* condition.

Since the major gradients of the background flow are in the radial direction (x direction in the simulation cube), the same concern does not apply to the y boundaries, however they can still affected by another problem. If the disparity between the smooth background state and the flow near the boundary is large, the simulated flow can still be adversely affected. In particular, the fixed condition at the boundary means that if some volume of gas flows towards that boundary but does not approximately match the conditions there, it may either be accelerated as it leaves the grid, causing mass further inside the simulation volume to be similarly accelerated into the prematurely evacuated volume, or it may be decelerated, effectively 'piling up' at the boundary and perhaps reentering the flow.

We have closely monitored the flow in our simulations for consequences of this effect and have observed it in only one (labeled *tm05* in table 1 above). We believe that the failure of this simulation is due primarily to the fact that the assumed background temperature was very low. As a consequence the Jeans wavelength of the mass in the grid became roughly comparable to the linear dimension of the simulation cube itself. As the planet drew additional mass into its influence, the perturbation on the local potential grew as well and further amplified the effect. The conditions just inside the boundary were then no longer similar to those just outside it and violated our smooth background assumption, resulting in matter turning back into the simulation volume and perturbing the evolution still further. A separate simulation, neglecting the local disk self gravity, did not suffer from this defect, and we discuss it in section 4.4.2 below as a more physically realistic alternative to simulation *tm05*, with a nearly identical physical model to its higher temperature cousins.

ACKNOWLEDGMENTS

We thank the anonymous referee for generous suggestions to improvement the manuscript. We also thank G. D'Angelo for his comments, which we used to clarify a number of the arguments made herein. We acknowledge the support of the University of Edinburgh Development Trust. The computations reported here were performed using the UK Astrophysical Fluids Facility (UKAFF) using time allocations during 2003-2004, which also provided financial support to AFN. Part of this work was carried out under the auspices

of the National Nuclear Security Administration of the U.S. Department of Energy at Los Alamos National Laboratory under Contract No. DE-AC52-06NA25396, for which this is LA-UR-12-26434.

REFERENCES

Alibert, Y., Mordasini, C., Benz, W. 2004 A&A 417, L25
Ayliffe, B. A., Bate, M. R., 2009, MNRAS, 393, 49 (AB09)
Balbus, S. A., Hawley, J. F., Stone, J. M., 1996, ApJ, 467, 76
Bate, M. R., Lubow, S. H., Ogilvie, G. I., Miller, K. A., 2003, MNRAS, 341, 213
Beckwith, S. V. W., Sargent, A. I., Chini, R. S. & Güsten, R., 1990, AJ, 99, 924
Boss, A.P., 1995, Science, 267, 360
Binney, J., Tremaine, S., 1987, Galactic Dynamics, Princeton University Press: Princeton
Ciesla, F. J. & Hood, L. L 2002, Icarus, 158, 281
Colella P., Woodward, P. R., 1984, J. Comp. Phys., 54, 174
D'Angelo, G., Henning, T., Kley, W., 2002, A&A, 385, 647
D'Angelo, G., Henning, T., Kley, W., 2003, ApJ, 586, 540
D'Angelo, G., Kley, W., Henning, T., 2003, ApJ, 599, 548
Desch, S. J., Connolly, H. C. Jr., Meteoritics & Planetary Science, 37, 187
Durisen R. H., Boss, A. P., Mayer, L., Nelson, A. F., Quinn, T. & Rice, W. K. M. 2007, In Protostars and Planets 5, p607-622, ed. Reipurth, B., Jewitt, D. & Keil, K. University of Arizona Press:Tucson
Foglizzo, T., Ruffert, M., 1999, A&A 347, 901
Goldreich, P., Lynden-Bell, D., 1965 MNRAS, 130, 7
Haisch, K. E., Lada, E. A., Lada, C. J., 2001, ApJL, 553, 153
Harker, D. E. & Desch, S. J. 2002, ApJ 565, 109
Hawley, J. F., Gammie. C. F., Balbus, S. A., 1995, ApJ, 440, 742
Helled, R., Podolak M., Kovetz, A., 2008 Icarus, 195, 863
Hubickyj, O., Bodenheimer, P., Lissauer, J. J., 2005, Icarus, 179, 415
Iida, A, Nakamoto, T. & Susa, H. 2001, Icarus, 153, 430
Jones, R. H., Lee, T., Connolly, H. C. Jr., Love, S. G. & Shang, H. 2000, In Protostars and Planets IV, pp. 927-962, ed. Mannings, V., Boss, A. P. & Russell, S. S., University of Arizona Press: Tucson
Lissauer, J. J., Hubickyj, O., D'Angelo, G., Bodenheimer, P., 2009, Icarus, 199, 338
Lubow, S. H. Seibert, M., Artymowicz, P., 1999, ApJ, 526, 1001
Machida, M. N., Kokubo, E., Inutsuka, S., Matsumoto, T. 2008, ApJ, 685, 1220
Masset, F., PhD Thesis, University of Paris
Miyoshi, K., Takeuchi, T., Tanaka, H., Ida, S., 1999, ApJ, 516, 451
Nelson, A. F., Benz, W., Adams, F. C., Arnett, W. D., 1998, ApJ, 502, 342
Nelson, A. F., Benz, W., Ruzmaikina, T. V., 2000, ApJ, 529, 357
Nelson, A. F., Benz, W., 2003, ApJ, 589, 556
Palme, H., Boynton, W. V., in Protostars and Planets III, ed. Lunine, J. I., Levy, E. University of Arizona Press: Tucson
Papaloizou, J. C. B., Nelson, R. P., 2006, A&A, 433, 247
Peplinski, A., Artymowicz, P., Mellema, G., 2008a, MNRAS, 386, 179
Peplinski, A., Artymowicz, P., Mellema, G., 2008b, MNRAS, 387, 1063
Pickett, B. K., Durisen, R. H., Davis, G. A., 1996, ApJ, 458, 714
Pickett, B. K., Cassen, P., Durisen, R. H., Link, R., 1998, ApJ, 504, 468
Pickett, B. K., Cassen, P., Durisen, R. H., Link, R., 2000, ApJ, 529, 1034
Pickett, B. K., Mejia, A. C., Durisen, R. H., Cassen, P. M., Berry, D. K., Link, R., 2003, ApJ, 590, 1060
Pollack, J. B., Hubickyj, O., Bodenheimer, P., Lissauer, J. J., Podolak, M., Greenzweig, Y., 1996, Icarus, 124, 62
Price, D. J.. 2012, J. Comp. Phys, 231, 759
Rafikov, R., 2006, ApJ, 648, 666
Ruffert, M., 1992, A&A, 265, 82
Ruffert, M., 1994, ApJ, 427, 342
Ruffert, M., 1997, A&A, 317, 793
Ruffert, M., 1999, A&A, 346, 861
Terquem, C., Heinemann, T., 2011, MNRAS, 418, 1928
Tanigawa, T., Ohtsuki, K., Machida, M. N., 2012, ApJ, 747, 47
Toman, J., Imamura, J. N., Pickett, B. K., Durisen, R. H., 1998, ApJ, 497, 370
Truelove, J. K., Klein, R. I., McKee, C. F., Holliman, J., H., Howell, L. H., Greenough, J. A., 1997, ApJL, 489, 179L
Ward, W. R. 1997, Icarus, 126, 261
Ward, W. R., Hahn, J., M., 2000, In Protostars and Planets 4, ed. Mannings, V., Boss, A. P. & Russell, S. S., University of Arizona Press: Tucson
Wuchterl, G., Guillot, T., Lissauer, J. J., 2000, In Protostars and Planets 4, ed. Mannings, V., Boss, A. P. & Russell, S. S., University of Arizona Press: Tucson